Journal of Hydrology 510 (2014) 259–279

Contents lists available at ScienceDirect

Journal of Hydrology

journal homepage: www.elsevier.com/locate/jhydrol

Potential evapotranspiration-related uncertainty in climate change impacts on river flow: An assessment for the Mekong River basin

J.R. Thompson [a,*], A.J. Green [a], D.G. Kingston [b]

[a] Wetland Research Unit, UCL Department of Geography, University College London, Gower Street, London WC1E 6BT, UK
[b] Department of Geography, University of Otago, PO Box 56, Dunedin, New Zealand

ARTICLE INFO

Article history:
Received 21 January 2013
Received in revised form 13 November 2013
Accepted 7 December 2013
Available online 15 December 2013
This manuscript was handled by Konstantine P. Georgakakos, Editor-in-Chief, with the assistance of Matthew McCabe, Associate Editor

Keywords:
Climate change
Uncertainty
Potential evapotranspiration
Mekong
MIKE SHE

SUMMARY

Six MIKE SHE models of the Mekong are developed, each employing potential evapotranspiration (PET) derived using alternative methods: Blaney–Criddle (BC), Hamon (HM), Hargreaves–Samani (HS), Linacre (LN), Penman (PN) and Priestley–Taylor (PT). Baseline (1961–1990) PET varies, with PT followed by HS providing the lowest totals, LN and BC the highest. The largest mean annual PET is over 1.5 times the smallest. Independent calibration of each model results in different optimised parameter sets that mitigate differences in baseline PET. Performance of each model is "excellent" (monthly NSE > 0.85) or "very good" (NSE: 0.65–0.85). Scenarios based on seven GCMs for a 2 °C increase in global mean temperature are investigated. Inter-GCM variation in precipitation change is much larger (in percentage terms by 2.5–10 times) than inter-GCM differences in PET change. Precipitation changes include catchment-wide increases or decreases as well as spatially variable directions of change, whereas PET increases for all scenarios. BC and HS produce the smallest changes, LN and HM the largest. PET method does impact scenario discharges. However, GCM-related uncertainty for change in mean discharge is on average 3.5 times greater than PET method-related uncertainty. Scenarios with catchment-wide precipitation increases (decreases) induce increases (decreases) in mean discharge irrespective of PET method. Magnitude of change in discharge is conditioned by PET method; larger increases or smaller declines in discharge result from methods producing the smallest PET increases. Uncertainty in the direction of change in mean discharge due to PET method occurs for scenarios with spatially variable precipitation change, although this is limited to few gauging stations and differences are relatively small. For all scenarios, PET method-related uncertainty in direction of change in high and low flows occurs, but seasonal distribution of discharge is largely unaffected. As such, whilst PET method does influence projections of discharge, variation in the precipitation climate change signal between GCMs is a much larger source of uncertainty.

1. Introduction

The projected impacts of climate change on the global hydrological cycle will have potentially significant implications for water resources (Bates et al., 2008; Gosling et al., 2011b; Gosling, 2012) and aquatic ecosystems (Poff et al., 2002; Matthews and Quesne, 2009). Hydrological impacts of climate change are commonly assessed by forcing a hydrological model with climate projections derived from General Circulation Models (GCMs) that are, in turn, forced with emissions scenarios. This approach has been used for global-scale assessments (Arnell, 2003; Nohara et al., 2006; Gosling et al., 2010; Arnell and Gosling, 2013), at regional (Arnell, 1999a) and national scales (Andréasson et al., 2004), and for individual catchments ranging in size from major river basins (Conway and Hulme, 1996; Nijssen et al., 2001) to medium and small sized catchments (Chun et al., 2009; Thompson et al., 2009, Thompson, 2012).

Uncertainty is associated with each stage of climate change hydrological impact assessments (Nawaz and Adeloye, 2006; Gosling et al., 2011a). There is uncertainty connected to the definition of greenhouse gas emissions scenarios with which GCMs are forced. Climate model structural uncertainty, which results from the different approaches used to represent the climate system within different GCMs, may lead to variable climate projections for the same emissions scenario. Downscaling of GCM projections to finer spatial and temporal scales for hydrological modelling is another source of uncertainty (e.g. Prudhomme and Davies, 2009).

A final source of uncertainty that in comparison to GCM-related uncertainty has received relatively little attention (Prudhomme

* Corresponding author. Tel.: +44 207 679 0589; fax: +44 0207 679 0565.
E-mail addresses: j.r.thompson@ucl.ac.uk (J.R. Thompson), amanda.green.09@ucl.ac.uk (A.J. Green), daniel.kingston@geography.otago.ac.nz (D.G. Kingston).

0022-1694
http://dx.doi.org/10.1016/j.jhydrol.2013.12.010

and Davies, 2009) is related to the hydrological models that translate climate scenarios to hydrological impacts (Gosling et al., 2011a). Research suggests, however, that this source of uncertainty may not be negligible (e.g. Dibike and Coulibaly, 2005; Haddeland et al., 2011; Hagemann et al., 2012; Thompson et al., 2013a). Hydrological models range from global models (e.g. Döll et al., 2003; Gosling and Arnell, 2011), through lumped or semi-distributed catchment models (e.g. Arnold et al., 1998), to fully distributed, physically based models (e.g. Refsgaard et al., 2010).

Hydrological model-related uncertainty may become evident when different hydrological models are applied to the same catchment. Although the models may produce equally acceptable results for an observed baseline period, they may subsequently respond differently when forced with the same GCM projections (Haddeland et al., 2011). For example, Gosling et al. (2011a) demonstrated differences in simulated discharge for the same set of climate change scenarios from catchment models and a global hydrological model for six river basins around the world, with changes in mean runoff varying by up to 25%. Thompson et al. (2013a) extended this analysis for the Mekong by developing a second catchment hydrological model (using MIKE SHE) and comparing results with the earlier catchment model (SLURP; Kingston et al., 2011) and the Mac-PDM.09 global model. Although in most cases the direction of change in mean discharge was the same for the different models for the same climate scenario, the magnitude of change varied. In particular, the global model projected increases in discharge at some upstream gauging stations that were three to five times as large as those for the catchment models. A possible explanation for these differences is the different potential evapotranspiration (PET) methods employed by the three models.

Previous research has demonstrated that different PET methods can produce very different climate change signals, with implications for assessments of the impacts of climate change on water resources (e.g. Arnell, 1999b; Kay and Davies, 2008; Bae et al., 2011). Kingston et al. (2009) demonstrated different PET climate change signals on a global basis using six alternative PET methods. PET-related uncertainty was of a similar magnitude or, in some cases, greater than GCM-related uncertainty for individual methods. Using a simple latitudinally averaged aridity index, it was shown that different PET methods could influence the projected direction of change in global water availability. Gosling and Arnell (2011) demonstrated large differences in runoff when two alternative PET methods, Penman–Monteith and Priestley–Taylor, were used within Mac-PDM.09. These differences varied depending on location; higher runoff was generated using the second PET method in relatively dry regions, whilst negative anomalies resulted for wetter regions. Bae et al. (2011) used three alternative semi-distributed catchment models and different PET methods to simulate climate change scenarios for a medium sized catchment (c. 7000 km^2) in central South Korea. Results showed that the different PET methods impacted runoff changes, with the magnitude of PET-related differences varying between hydrological models and season.

The PET method(s) employed within a hydrological model may, therefore, be a specific source of hydrological model-related uncertainty but one that has been relatively under-investigated (Prudhomme and Williamson, 2013). There are over 50 different PET methods that could be employed within hydrological models (Lu et al., 2005). PET method selection may be influenced by a number of factors. Where a hydrological model calculates PET internally, the method will depend upon those incorporated within the model (Bae et al., 2011). Data availability may also exert an important influence since different PET methods require different meteorological variables. This may have important implications for climate change assessments since less confidence is placed in GCM simulations of some variables such as cloud cover and vapour pressure compared to others, most notably temperature (Randall et al., 2007). Similarly, other variables, such as wind speed and net radiation, are typically less reliable in the gridded datasets often used for baseline simulations (e.g. Haddeland et al., 2011) due to measurement difficulties and the relatively limited number of observations (New et al., 1999). Although many large-scale (global) hydrological models use either the Penman–Monteith or Priestley–Taylor methods, these decisions are often based on the theoretically more realistic nature of these methods as opposed to a large-scale validation of their output (although Sperna Weiland et al. (2012) is an exception).

The current study investigates the implications of using alternative PET methods for discharge projections for the Mekong River of southeast Asia. This is achieved using the MIKE SHE model developed by Thompson et al. (2013a) and its recalibration for five additional PET methods. Subsequently each of these models are used to simulate climate change scenarios based on projections from seven GCMs for a 2 °C increase in global mean temperature.

2. Methods

2.1. The Mekong catchment

The Mekong is the largest river in southeast Asia. It is the world's eighth largest in terms of annual discharge (475 km^3), 12th longest (c. 4350 km) and 21st largest by drainage area (795,000 km^2) (Kiem et al., 2008). Rising in the Tibetan Highlands at an elevation of over 5100 m, it passes through six countries before discharging into the South China Sea via the distributaries of the Mekong Delta (Fig. 1).

The dominant climatic influence is the Asian monsoon. Rains begin in mid-May and extend into early-October, with over 90% of annual precipitation falling within this period (Kite, 2001). Annual precipitation ranges from under 1000 mm on the Korat Plateau of eastern Thailand to over 3200 mm in mountainous parts of Laos. Snow is restricted to parts of the Tibetan Highlands and Yunan and covers approximately 5% of the catchment between November and March. Snowmelt contributes to the initial rise of the annual flood within the upper catchment (the Lancang; Kiem et al., 2005). River discharge begins to rise in May and peaks between August and October. The subsequent recession continues until March–April.

The upper catchment is characterised by narrow, steep gorges. Land cover is primarily tundra and montane semi-desert (Kite, 2001). Further downstream, natural vegetation is dominated by evergreen and deciduous forest (Ishidaira et al., 2008). Rapid economic development, growing populations and conflicts have, however, caused widespread deforestation in favour of agriculture (Nobuhiro et al., 2008; Lacombe et al., 2010). Additional pressures stem from competition for water, contamination by agriculture, industry and settlements, and unsustainable use of resources such as fisheries. Dams have been implicated in changes in discharge, sediment flows and fisheries (Hapuarachchi et al., 2008; Li and He, 2008; Kummu et al., 2010; Wang et al., 2011). Future dams will exacerbate these changes (Stone, 2010).

2.2. The MIKE SHE model of the Mekong

MIKE SHE is a modelling system that simulates the major processes of the land phase of the hydrological cycle (Graham and Butts, 2005). It has been employed in small catchments (Al Khudhairy et al., 1999; Thompson et al., 2004; Thompson, 2012), catchments of hundreds or thousands of km^2 (Feyen et al., 2000; Huang et al., 2010; Singh et al., 2010, 2011) and major international river basins (Andersen et al., 2001; Stisen et al., 2008). Although often

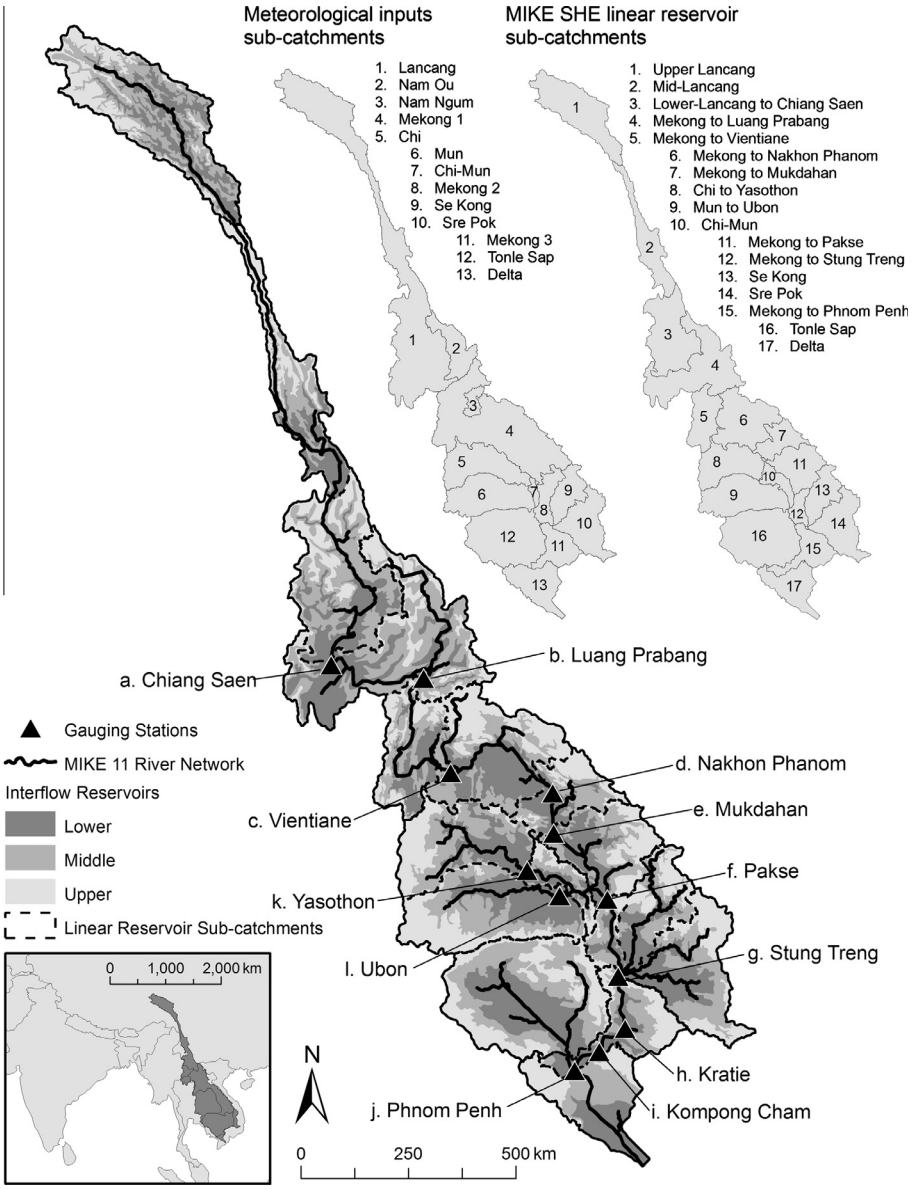

Fig. 1. The Mekong catchment and its representation within the MIKE SHE model including the distribution of linear reservoir sub-catchments, interflow reservoirs and meteorological inputs. The gauging stations within the MIKE 11 river network that were used for calibration and validation are also indicated.

described as fully distributed and physically based, after decades of development it includes a range of process descriptions, some of which are conceptual and semi-distributed.

Thompson et al. (2013a) provide a detailed description of the Mekong MIKE SHE model. Since an aim of this earlier study was to evaluate inter-hydrological model uncertainty, the model utilised, as far as possible, the same data, and hence the same meteorological input sub-catchments, as an earlier model created using the Semi-distributed Land Use-based Runoff Processes (SLURP, v.12.7) model (Kite, 1995, 2001; Kingston et al., 2011). Table 1 summarises the components of the MIKE SHE model and the data employed within them. Overland flow is calculated using a finite-difference approach for the two-dimensional Saint–Venant equations (Graham and Butts, 2005). The two-layer water balance method (e.g. Yan and Smith, 1994) is used for the unsaturated zone. For the saturated zone, the conceptual, semi-distributed, linear reservoir method is employed. With its lower data requirements and reduced model execution times compared to physically based solutions this method is particularly useful for large catchments (e.g. Andersen et al., 2001; Stisen et al., 2008).

Precipitation, temperature and PET were spatially distributed according to the 13 sub-catchments employed within the SLURP model (Fig. 1). However, in order to aid calibration the Mekong was instead divided into 17 linear reservoir sub-catchments (Fig. 1). These were based on the locations of (i) the 12 gauging stations used for model calibration/validation, (ii) major tributaries and (iii) large changes in topographic characteristics. Results from the Tonle Sap and Delta sub-catchments were not analysed due to a lack of observed discharge records. Each linear reservoir sub-catchment was divided into three interflow reservoirs based on topography. Two baseflow reservoirs, representing faster and slower baseflow storage, were specified for each sub-catchment. Exchanges between reservoirs, and ultimately the MIKE 11 hydraulic model, were controlled by time constants.

MIKE SHE's computational grid was set to 10 km × 10 km, following experiments showing simulated discharge varied little with grid sizes of between 1 km and 20 km (see also Vázquez et al., 2002; Thompson, 2012). Hypsometric curves for the resampled and original topography are very similar, as are the relative importance of the different soil and land use categories, suggesting that

Table 1
Summary of key data employed within each component of the coupled MIKE SHE/MIKE 11 model of the Mekong.

Model component	Key inputs	Data sources/derivation
Model domain	Catchment extent	Derived using the USGS GTOPO30 DEM (Kite, 2000)
Topography	Topography	Extracted from the USGS GTOPO30 DEM
Land use/vegetation	Vegetation distribution	Spatial distribution of nine land cover classes derived from the USGS Global Land Cover Characterization dataset
	Leaf Area indices	Kite (2000)
	Root depths	Kelliher et al. (1993), Jackson et al. (1996), DHI (2009) vegetation properties file
Overland flow: modelled using the 2D finite-difference method	Manning's M for overland flow resistance	Spatially distributed according to land cover. Values taken from the literature (Chow, 1959; Thompson et al., 2004; Vieux, 2004; Sahoo et al., 2006; Thompson, 2012)
Unsaturated zone: modelled using the two-layer water balance method	Soil textural classes	Spatial distribution of four textural classed derived from the FAO Digital Soil Map of the World (FAO, 1990)
	Soil hydraulic properties	Clapp and Hornberger (1978), Carsel and Parrish (1988), Marshall et al. (1996)
Saturated zone: modelled using the conceptual, linear reservoir method	Spatial distribution of sub-catchments	The catchment was divided into 17 groundwater sub-catchments (Fig. 1) based on: the locations of 12 gauging stations used for model calibration/validation, major tributaries and topography
	Spatial distribution of interflow reservoirs	Each sub-catchment was divided into three interflow reservoirs, based on topography
	Spatial distribution of baseflow reservoirs	Each sub-catchment was divided into an upper (faster) and a lower (slower) baseflow reservoir
Catchment meteorology: Precipitation, evapotranspiration and snowmelt modules	13 meteorological sub-catchments	Derived through topographic analysis of the USGS GTOPO30 DEM (Kite, 2000)
	Precipitation, potential evapotranspiration (PET) and temperature data	See text for meteorological data sources
MIKE 11 one-dimensional hydraulic model for simulating channel flow	Plan of the main river channels	Derived through topographic analysis of the USGS GTOPO30 DEM (Kite, 2000)
	Cross-sections for different stream orders	Established using surveyed cross-sections (Shopea, 2003; Mekong River Commission: http://ffw.mrcmekong.org/) and stream width measurements taken in Google Earth Pro
	Manning's n for bed resistance	Chow (1959)

the larger grid size retains a good representation of catchment characteristics.

Channel flow was simulated using the one-dimensional hydraulic model, MIKE 11 (Havnø et al., 1995). A plan of the main river channels was derived from the USGS GTOPO30 DEM using the TOPAZ digital terrain analysis model (Garbrecht and Martz, 1997). Cross-sections for different stream orders were based on available surveyed cross-sections and remotely sensed imagery (Table 1). Dams were not included as many of the extant dams were completed after the calibration period. All MIKE 11 river branches were coupled to the MIKE SHE model, and so received exchanges from MIKE SHE in the form of overland flow, interflow and baseflow.

Gridded monthly precipitation totals were obtained from the University of Delaware global precipitation dataset (UDel; Legates and Willmott, 1990). Updated versions of these data (V1.01 and V1.02) compared to those employed by Thompson et al. (2013a) were used for the validation period (see below). Mean temperature data were derived from the CRU TS 3.0 dataset (Mitchell and Jones, 2005). Monthly data were spatially averaged for each of the 13 meteorological input sub-catchments and stochastically disaggregated to a daily resolution using a weather generator (Arnell, 2003; Todd et al., 2011). The number of $0.5^\circ \times 0.5^\circ$ grid cells used to obtain sub-catchment averages varies from 1 (Chi-Mun), to 83 (Lancang), with a mean of 21. The original MIKE SHE model used temperature based Linacre PET as adopted in the earlier SLURP model. Monthly gridded PET was calculated using climate variables obtained from the CRU TS 3.0 dataset. Monthly PET was then evaluated for each of the meteorological input sub-catchments. PET was distributed evenly through each month.

2.3. Alternative PET methods

In addition to the temperature-based Linacre (LN) PET (Dent et al., 1988; Schultz, 1989), five alternative methods were employed to calculate PET. They represent a sample of the methods commonly used within hydrological models and reflect varying data requirements. Blaney–Criddle (BC) and Hamon (HM) are both based on temperature and day-length, with the latter being employed within the WBM global hydrological model (Vörösmarty et al., 1998). Hargreaves–Samani (HS) uses mean, minimum and maximum temperature and extra-terrestrial solar radiation and is often used in situations where data are insufficient to calculate Penman or Penman–Monteith (Allen et al., 1998). These methods incorporate the meteorological variables that control evapotranspiration (net radiation, temperature, wind speed and vapour pressure) and are used in many hydrological models including the MacPDM global model (Arnell, 1999b). In the absence of detailed land cover information required to calculate crop reference ET according to the FAO-56 Penman–Monteith equation (Allen et al., 1998), the Penman (1948) PET (PN) method was used. Finally, Priestley–Taylor (PT) provides a simplification of the Penman/Penman–Monteith method based on net-radiation and temperature and is used in the WaterGAP hydrological model (Alcamo et al., 2007).

Data for each PET method were derived from the CRU TS 3.0 dataset with the exceptions of cloud cover (CRU TS 2.1) and wind speed (climatological values, since these data are not available within the CRU dataset). Monthly PET was calculated for each of the 268 grid cells covering the Mekong catchment. BC was calculated according to Brouwer and Heibloem (1986), PN according to Penman (1948) as expressed by Shuttleworth (1993), whilst HM and PT were calculated using Lu et al. (2005). HS was calculated following Hargreaves and Samani (1982). As described in Section 2.2, mean monthly PET for each meteorological input sub-catchment was evenly distributed through each month (post-calibration experiments using stochastically temporally distributed PET showed very little impact on simulated river flow). Time series of PET from each method were specified within separate MIKE SHE models so that, including the original model employing LN PET, six hydrological models were defined.

2.4. Model calibration and validation

The same calibration/validation procedures were employed for each MIKE SHE model, and were undertaken independently – the aim of calibration was to achieve equally good performance for each model. A baseline period of 1961–1990 was used for calibration and the shorter 1991–1998 period for validation. Observed discharge from 12 gauging stations was used for calibration (Fig. 1). Ten stations are on the main Mekong whilst two are on tributaries (the Chi and Mun). The length of records for three stations did not cover the complete calibration period, whilst discharge for Kratie was derived from records for Pakse using a linear regression model (Institute of Hydrology, 1988).

Calibration parameters were the time constants of the saturated zone's interflow and baseflow reservoirs, and in sub-catchments with large elevation ranges, the precipitation lapse rate. In a limited number of sub-catchments (discussed below), it was necessary to incorporate a dead storage proportion for the baseflow reservoirs. Thompson et al. (2013a) determined an appropriate snowmelt degree-day coefficient when calibrating their LN-based model for the Lancang at Chiang Saen (the one sub-catchment where snow regularly occurs). The same degree-day coefficient was used in the five other models.

Calibration was undertaken in a downstream sequence from Chiang Saen to Mukdahan, followed by the two tributaries (Yasothon and Ubon) and then from Pakse to Phnom Penh. Since there is a disconnect between daily meteorological inputs derived from monthly totals (mean for temperature) using a weather generator and observed discharge (Kingston et al., 2011), manual parameter modification was undertaken with observed and simulated discharge being aggregated to mean monthly flow (Thompson et al., 2013a). Model performance was assessed using the Nash–Sutcliffe coefficient (NSE, Nash and Sutcliffe, 1970), the Pearson correlation coefficient (r) and percentage deviation in simulated mean flow from observed mean flow (Dv; Henriksen et al., 2003). Classification of model performance based on Dv and NSE used the scheme of Henriksen et al. (2008). Following calibration, each model was run for the 1991–1998 validation period. Data for two gauging stations, Kompong Cham and Phnom Penh, were not available for this period, whilst the length of records for the remaining stations varied from the complete eight years to only three years.

Separate calibration of each of the six MIKE SHE models is a noteworthy aspect of this study. Previous studies of uncertainty in climate change impacts on discharge associated with PET method have avoided the issue of different baseline PET values affecting model performance by developing a baseline hydrological model employing a single PET method that is subsequently forced using PET delta factors (e.g. Kay and Davies, 2008). Whilst this could have been undertaken here, it would necessitate selection of a particular PET method for the baseline with choice of that method over another representing a further source of uncertainty. Other studies (e.g. Bae et al., 2011) have optimized their baseline hydrological model to a single PET method and then implemented different PET methods without further optimization. Although this has the advantage of meaning that baseline-scenario changes in discharge are not influenced by changes in parameter values, it means that a non-optimal hydrological model is used for all but one of the PET methods investigated. In demonstrating the impact on optimized model parameter values of using different PET methods this study presents a useful alternative to these two previous approaches.

2.5. Simulation of climate change

Future (monthly resolution) climate scenarios for precipitation, temperature and the other meteorological variables used by the different PET methods were derived for a 30 year period using the ClimGen spatial scenario generator (Arnell and Osborn, 2006). ClimGen employs the assumption that spatial patterns of climate change, expressed as change per unit of global mean temperature, are constant for a GCM. This permits the pattern of climate change for a given GCM to be scaled up and down in magnitude, enabling impacts of specific thresholds of global climate change to be investigated. Scenarios were generated for a prescribed increase in global mean temperature of 2 °C, the hypothesised threshold for 'dangerous' climate change (Todd et al., 2011), for seven GCMs: CCCMA CGCM31, CSIRO Mk30, IPSL CM4, MPI ECHAM5, NCAR CCSM30, UKMO HadGEM1 and UKMO HadCM3. They were selected from the CMIP-3 database (Meehl et al., 2007) for application within the QUEST-GSI project (Todd et al., 2011). These GCMs represent different future representations of global climate system features (e.g. Indian monsoon weakening/strengthening, magnitude of Amazon dieback).

The $0.5^\circ \times 0.5^\circ$ gridded scenario precipitation and temperature time series derived using ClimGen were averaged for each meteorological input sub-catchment and downscaled from monthly to daily resolution using a weather generator. Scenario PET was calculated for each $0.5^\circ \times 0.5^\circ$ grid square using the ClimGen outputs and the methods employed for the baseline period. Gridded PET was then averaged at the meteorological input sub-catchment scale. As for the baseline period, PET was evenly distributed on a daily basis through each month. Scenario PET was subsequently specified within the MIKE SHE models calibrated using the respective PET method. In this way a total of 42 scenario model runs were simulated (seven GCMs for each of the six hydrological models employing different PET methods).

3. Results

3.1. Baseline PET

Mean annual PET for the 1961–1990 baseline period for the six PET methods is shown for eight representative sub-catchments in Table 2 (top). The relative magnitude of PET from the different methods follows a general, but not wholly consistent, pattern in each sub-catchment. PT PET is the lowest in all sub-catchments except the Lancang, for which it is the second lowest (and HM the lowest). In upstream sub-catchments LN produces the largest annual PET followed by BC. Further downstream (from Mekong 2) this order is reversed whilst for the lowest sub-catchment (Mekong 3), HM PET is the second highest. With the exception of the Lancang and Mekong 3, HM PET provides the third highest totals in all sub-catchments. Annual HS PET is very similar to PN PET, which is to be expected given that the former is the preferred alternative to PN (or Penman–Monteith, Allen et al., 1998). With the exception of the Lancang, HS and PN are both lower than BC, HM and LN but higher than PT PET.

There is a relatively consistent spatial pattern in annual PET. With the exception of LN PET, the lowest totals occur over the Lancang. This is unsurprising given its higher elevation and lower temperatures (mean temperature is 11.2 °C compared to 24.3 °C for Mekong 1, Table 2 - bottom). Annual PET increases along the Mekong (Lancang – Mekong 1 – Mekong 2 – Mekong 3) for all methods except LN (highest PET is for Mekong 1). Increasing PET in this direction echoes higher temperatures, although beyond Mekong 1 temperature variations are relatively small (Table 2 – bottom). The Chi and, in particular, the Mun have the highest mean annual temperatures and experience the highest mean annual PET for most methods.

Mean monthly PET derived for 1961–1990 using the six methods is shown in Fig. 2 for four representative sub-catchments. Generally higher PET for the temperature-based methods (except HM

Table 2
Mean annual baseline potential evapotranspiration for each PET method, precipitation (mm) and temperature (°C) and changes (% for precipitation and PET, °C for temperature) for the 2 °C, seven GCM climate change scenarios for representative sub-catchments within the Mekong catchment. Numbers in brackets refer to the meteorological input sub-catchments identified in Fig. 1. Italicised values indicate negative changes compared to the baseline.

Parameter	Scenario	Lancang (1)	Mek. 1 (4)	Chi (5)	Mun (6)	Mek. 2 (8)	Se Kong (9)	Sre Pok (10)	Mek. 3 (11)
Baseline PET (mm)	BC	1337.9	1922.1	2032.4	2057.7	2001.4	1943.0	1922.3	2041.2
	HM	778.1	1631.6	1860.6	1905.9	1776.5	1654.6	1619.2	1866.6
	HS	1130.4	1516.3	1695.3	1726.1	1564.4	1489.5	1477.5	1652.6
	LN	1765.6	1923.0	2363.6	2336.5	1813.0	1728.5	1695.9	1770.3
	PN	1111.5	1510.3	1713.7	1715.1	1585.5	1506.7	1480.2	1692.0
	PT	954.8	1352.0	1468.5	1487.6	1392.1	1374.3	1388.3	1574.9
CCCMA PET (% change)	BC	7.8	4.4	4.4	4.4	4.2	4.4	4.6	4.4
	HM	14.6	11.0	11.3	11.4	10.6	11.0	11.2	11.3
	HS	7.2	4.2	4.1	4.3	4.4	4.7	4.9	4.8
	LN	11.7	12.3	13.1	12.7	12.5	12.7	12.3	12.5
	PN	3.9	5.7	6.3	6.7	6.1	6.0	6.6	6.1
	PT	9.8	7.2	7.5	7.9	8.4	8.4	9.2	7.1
CSIRO PET (% change)	BC	9.2	5.5	5.1	5.0	4.8	4.8	4.8	4.8
	HM	17.6	13.8	13.4	13.1	12.4	12.2	12.0	12.5
	HS	10.1	8.0	6.9	6.6	7.3	7.5	7.3	7.4
	LN	14.6	15.7	15.9	15.2	15.2	14.9	14.2	14.3
	PN	10.4	11.4	10.1	9.8	9.9	9.4	8.6	9.2
	PT	11.5	10.1	9.1	8.9	10.6	10.3	9.5	8.5
HadCM3 PET (% change)	BC	8.8	5.7	5.4	5.3	5.2	5.3	5.3	5.2
	HM	16.4	14.0	13.8	13.6	13.3	13.2	13.2	13.5
	HS	7.8	5.3	5.2	5.5	6.3	6.6	7.1	7.6
	LN	12.9	13.9	13.3	13.2	14.7	14.8	14.8	15.1
	PN	1.8	7.7	7.7	8.7	8.3	8.8	10.0	9.9
	PT	9.7	7.5	6.6	7.3	7.5	8.4	9.2	7.0
HadGEM1 PET (% change)	BC	8.7	4.6	4.0	4.0	4.3	4.6	4.7	4.5
	HM	16.1	11.5	10.2	10.3	10.9	11.5	11.6	11.7
	HS	8.1	4.4	3.8	3.9	4.5	4.9	5.0	4.9
	LN	12.4	12.1	10.3	10.3	12.4	13.0	12.7	12.5
	PN	9.1	7.3	5.8	6.5	6.7	6.7	7.0	7.0
	PT	7.8	5.1	4.5	5.5	5.8	5.6	6.2	5.2
IPSL PET (% change)	BC	9.9	5.5	4.9	4.7	4.7	4.7	4.5	4.4
	HM	19.2	14.1	13.0	12.4	12.1	11.9	11.1	11.4
	HS	9.4	5.4	4.7	4.6	5.0	5.0	4.8	4.8
	LN	15.9	15.7	15.3	14.2	14.3	13.9	12.8	13.2
	PN	11.9	11.1	9.9	9.1	9.3	7.7	5.6	7.2
	PT	12.3	9.0	8.3	8.0	9.1	7.8	6.2	6.4
MPI PET (% change)	BC	9.1	5.1	4.7	4.7	4.6	4.7	4.7	4.6
	HM	17.1	12.8	12.4	12.3	11.8	11.8	11.7	12.0
	HS	8.5	5.0	4.6	4.7	4.9	5.0	5.1	5.1
	LN	13.6	13.6	13.3	12.9	13.4	13.5	13.1	13.2
	PN	9.7	7.1	6.0	6.3	5.7	5.0	4.8	5.3
	PT	11.6	6.2	5.2	5.7	6.3	5.9	5.9	4.9
NCAR PET (% change)	BC	8.1	4.4	4.1	4.1	4.0	4.0	4.0	3.8
	HM	15.1	10.7	10.6	10.5	10.0	9.9	9.8	9.8
	HS	5.3	2.8	3.6	3.8	3.8	3.4	2.9	2.7
	LN	11.3	10.9	11.1	10.6	11.4	11.1	10.7	10.3
	PN	5.5	5.1	5.3	5.6	5.1	3.8	3.8	4.4
	PT	7.1	4.4	4.6	5.4	5.9	5.1	5.5	5.2
Precipitation (mm/% change)	Baseline	1052.8	1855.8	1272.3	1313.6	2213.2	2432.5	2055.3	1870.3
	CCCMA	10.1	10.2	12.3	10.2	8.4	5.2	1.9	5.3
	CSIRO	*−4.6*	*−4.6*	*−3.3*	*−2.9*	*−2.8*	*−2.8*	*−2.9*	*−1.3*
	HadCM3	10.1	1.0	*−0.1*	*−0.4*	*−1.1*	*−2.1*	*−4.5*	*−3.0*
	HadGEM1	5.9	*−3.7*	*−6.1*	*−4.8*	*−1.2*	2.9	3.9	1.0
	IPSL	*−5.2*	*−1.1*	*−0.1*	*−0.1*	0.6	*−0.4*	1.3	*−0.4*
	MPI	3.6	7.0	10.2	10.3	8.8	6.6	7.6	12.2
	NCAR	8.5	9.1	5.0	3.5	1.9	3.5	3.7	5.3
Temperature (°C/°C change)	Baseline	11.20	24.33	26.76	27.21	26.00	24.72	24.33	26.95
	CCCMA	2.29	1.87	1.97	1.99	1.85	1.90	1.93	1.96
	CSIRO	2.69	2.30	2.27	2.22	2.09	2.04	2.01	2.13
	HadCM3	2.54	1.97	1.80	1.82	1.90	1.98	1.98	2.03
	HadGEM1	2.54	1.97	1.80	1.82	1.90	1.98	1.98	2.03
	IPSL	2.88	2.33	2.19	2.11	2.07	2.02	1.89	1.97
	MPI	2.66	2.15	2.11	2.11	2.02	2.01	2.00	2.06
	NCAR	2.37	1.87	1.86	1.84	1.76	1.71	1.69	1.71

for the Lancang) is demonstrated. Lower PET occurs for the PN and PT methods. Some methods (BC, HM) have a consistent June–August peak whilst in others (e.g. PN, PT) the seasonal peak is earlier (March–April). Seasonality declines in a downstream direction. For the Lancang maximum monthly PET is, on average, 2.4 times the minimum. This reduces to 1.6 for Mekong 1 and 1.4 for Mekong 3.

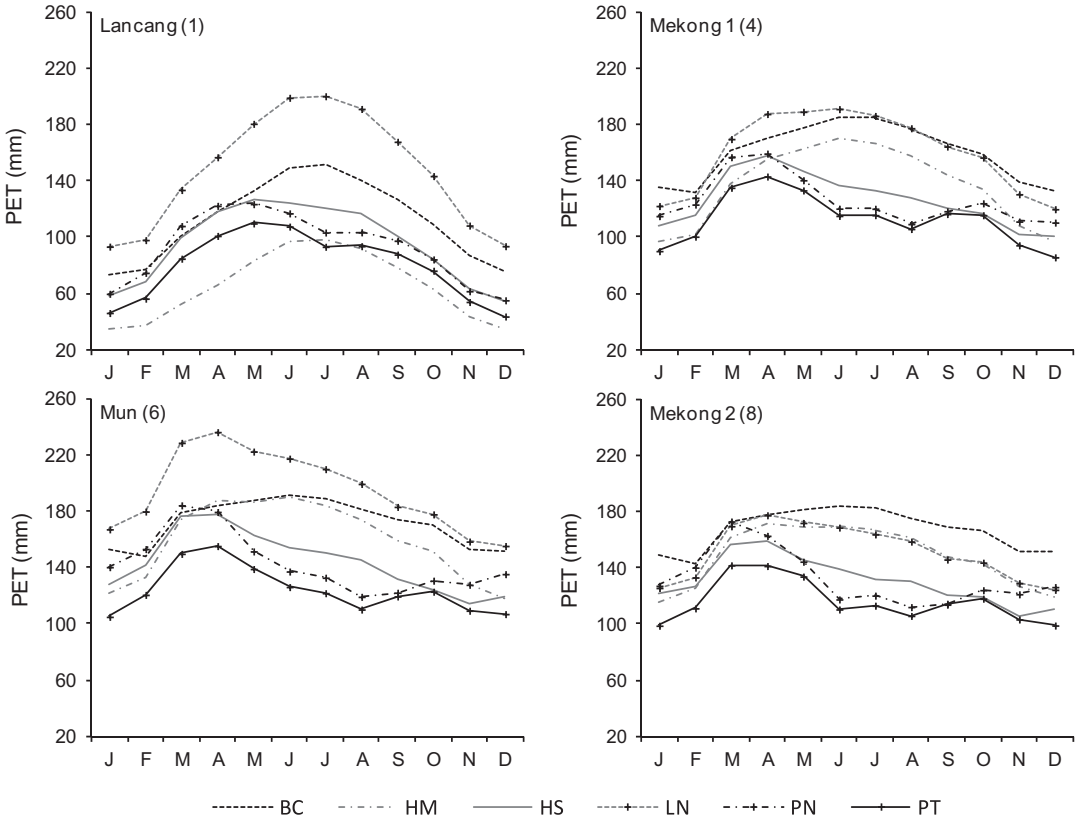

Fig. 2. Mean monthly baseline (1961–1990) potential evapotranspiration for each PET method for four representative sub-catchments. Numbers in brackets refer to the meteorological input sub-catchments identified in Fig. 1.

3.2. Model calibration

Table 3 summarises the optimised values of the baseflow time constants, precipitation lapse rates in sub-catchments with large elevation ranges and, for some sub-catchments, dead storage proportions. Interflow reservoir time constants were also varied during calibration, but differences between models were relatively small. There is no consistency in the relative magnitudes of the baseflow time constants between the models. In contrast, models employing PET methods associated with the highest baseline PET required the largest precipitation lapse rates. For example, LN and HM PET provide the largest and smallest mean annual baseline PET over the Lancang and result in the largest (2.16) and smallest (0.26) optimal precipitation lapse rates, respectively. The use of single or multiple precipitation lapse rates as a calibration term has been adopted elsewhere (e.g. Yu et al., 2011; Ji and Luo, 2013). The values in Table 3 are within the range of those previously reported in mountainous regions (e.g. Immerzeel et al., 2012a,b). Variable lapse rates for sub-catchments with large elevation ranges mitigates the differences between PET methods.

Observed and simulated mean monthly discharges from the six MIKE SHE models for the baseline period are shown in Fig. 3. The very narrow range of simulated river regimes, especially for the ten gauging stations on the main Mekong, illustrates the very similar performance of the models. Good model performance for the main Mekong is further demonstrated in Table 4. As reported by Thompson et al. (2013a) for the LN PET model, out of the 24 Dv and NSE model performance statistics, 20 were classified as "excellent" according to the scheme of Henriksen et al. (2008). This scheme was originally based on comparisons of daily observed and simulated discharge. Higher NSE values are to be expected when aggregating to monthly mean discharges. Increasing the lower boundary of the "excellent" class for NSE to 0.9 still results in half of the models (HS, PM, PT) being classified as "excellent" for all the stations on the main Mekong. Even if the lower boundary of the "very good" class is increased to 0.85, the performance of all the other models falls into this category. Relatively poor performance is achieved for Phnom Penh, a station with a shorter observed discharge record. Although NSE is classified as "excellent" for all six models, the overestimation of mean discharge results in Dv being classed as "very good" (two models) or "fair" (four models). Although an equivalent classification for the correlation coefficient (r) is not employed, the value of this statistic is above or very close to 0.95 for ten of the 12 stations.

The two stations with lower values of r (Yasothon and Ubon) also have lower values of NSE that are, in most cases, classified as "fair" ("poor" for Yasothon for BC and LN). Thompson et al. (2013a) reported that it was not possible to raise peak discharges for these stations without also raising discharge during the reasonably well-reproduced annual rise and recession. This would cause Dv to increase substantially. Calibration therefore focussed on matching observed and simulated mean flow (i.e. Dv values close to 0), and hence annual contributions from these tributaries to the Mekong. This necessitated the use of dead storage terms within the MIKE SHE linear reservoirs (Table 3). The same issue was experienced in the calibration of the Mekong at Vientiane (sub-catchment 5), adjacent and to the north of the Chi.

Explanations for flow overestimation without dead storage could lie with the meteorological inputs. Hughes et al. (2011) identified geographically isolated extreme rainfall within the CRU TS 3.0 dataset over the Okavango catchment, southern Africa that could potentially be attributed to anomalies within station data used in its derivation. This impacted hydrological model calibration and was addressed, at least in part, using UDel precipitation.

Table 3
Final calibration parameter values for the six MIKE SHE models employing different PET methods. Numbers in column headings refer to the MIKE SHE linear reservoir sub-catchments identified in Fig. 1.

Parameter	PET	1	2	3	4	5	6	7	8	9	10	11	12	13	14	15
Precipitation lapse rate (%/100 m)	BC	1.38	1.38	1.38	4.00	0.00	9.90	0.00	0.00	1.80	0.00	0.00	0.00	0.00	0.00	0.00
	HM	0.26	0.26	0.26	0.50	0.00	8.20	0.00	0.00	0.00	0.00	0.00	0.00	0.00	0.00	0.00
	HS	0.85	0.85	0.85	0.70	0.00	6.50	0.00	0.00	0.00	0.00	0.00	0.00	0.00	0.00	0.00
	LN	2.16	2.16	2.16	5.80	0.00	8.48	0.00	0.00	3.47	0.00	0.00	0.00	0.00	0.00	0.00
	PN	0.68	0.68	0.68	0.00	0.00	4.60	0.00	0.00	0.00	0.00	0.00	0.00	0.00	0.00	0.00
	PT	0.45	0.45	0.45	0.00	0.00	3.60	0.00	0.00	0.00	0.00	0.00	0.00	0.00	0.00	0.00
Time constant for baseflow reservoir 1 (days)	BC	150	150	150	90	110	75	111	178	135	90	20	40	20	20	150
	HM	100	100	100	55	130	50	121	180	130	100	30	50	30	30	100
	HS	135	135	135	55	125	80	100	170	135	105	50	55	65	70	175
	LN	145	145	145	75	120	55	113	175	105	95	55	30	20	20	105
	PN	115	115	115	80	127	45	119	179	138	115	75	60	90	90	150
	PT	105	105	105	90	140	43	122	185	145	140	70	55	70	70	180
Dead storage fraction for baseflow reservoir 1	BC	0.00	0.00	0.00	0.00	0.00	0.00	0.00	0.08	0.00	0.00	0.00	0.00	0.00	0.00	0.00
	HM	0.00	0.00	0.00	0.00	0.00	0.00	0.00	0.20	0.00	0.00	0.00	0.00	0.00	0.00	0.00
	HS	0.00	0.00	0.00	0.00	0.00	0.00	0.00	0.37	0.00	0.00	0.00	0.00	0.00	0.00	0.00
	LN	0.00	0.00	0.00	0.00	0.00	0.00	0.00	0.00	0.00	0.00	0.00	0.00	0.00	0.00	0.00
	PN	0.00	0.00	0.00	0.00	0.00	0.00	0.00	0.46	0.00	0.00	0.00	0.00	0.00	0.00	0.00
	PT	0.00	0.00	0.00	0.00	0.00	0.00	0.00	0.44	0.00	0.00	0.00	0.00	0.00	0.00	0.00
Time constant for baseflow reservoir 2 (days)	BC	750	640	880	700	900	160	131	400	185	141	60	350	120	120	450
	HM	725	630	883	893	700	150	250	440	190	121	70	500	100	100	400
	HS	760	655	900	580	850	150	180	300	195	150	90	550	160	170	600
	LN	740	645	880	550	600	90	121	530	149	135	80	300	110	110	390
	PN	745	690	890	550	610	160	231	380	180	200	100	330	285	285	380
	PT	770	680	910	545	650	170	240	450	155	220	110	400	300	300	500
Dead storage fraction for baseflow reservoir 2	BC	0.00	0.00	0.00	0.00	0.40	0.00	0.00	1.00	0.00	0.00	0.00	0.00	0.00	0.00	0.00
	HM	0.00	0.00	0.00	0.00	0.55	0.00	0.00	0.96	0.05	0.00	0.00	0.00	0.00	0.00	0.00
	HS	0.00	0.00	0.00	0.00	0.55	0.00	0.00	0.96	0.44	0.00	0.00	0.00	0.00	0.00	0.00
	LN	0.00	0.00	0.00	0.00	0.30	0.00	0.00	0.90	0.00	0.00	0.00	0.00	0.00	0.00	0.00
	PN	0.00	0.00	0.00	0.00	0.80	0.00	0.00	0.93	0.59	0.00	0.00	0.00	0.00	0.00	0.00
	PT	0.00	0.00	0.00	0.00	0.95	0.00	0.00	1.00	0.68	0.00	0.00	0.00	0.00	0.00	0.00

For the Chi and Mun discharge overestimation could result from elevated precipitation within the UDel dataset. Mean annual sub-catchment precipitation (Table 2) exceeds reported estimates of less than 1000 mm for the Korat Plateau (Kite, 2001). Similarly, the relatively small sub-catchment above Vientiane (sub-catchment 5) falls within the large Mekong 1 meteorological input sub-catchment that has a mean annual precipitation of over 1800 mm (Table 2) whilst Kiem et al. (2008) present data that suggest lower (1200–1500 mm) annual totals.

Overestimation of discharge without dead storage could also be related to land use. Of all the sub-catchments, the Chi and the Mun are the most agricultural with extensive areas of irrigation, some dating back to the 1950s and 1960s (Floch and Molle, 2007). Without detailed information on the representativeness of the gridded precipitation dataset and on irrigation abstractions, the application of dead storage in these few sub-catchments was considered justified in order to match observed and simulated annual contributions to the main Mekong. Furthermore, the mean annual water balance was assessed for all the gauging stations along the main Mekong to ensure that dead storage was not unduly large. As a percentage of precipitation, change in subsurface storage (including both the saturated and unsaturated zones) is no more than 5% of precipitation (mean 1.5%) and 9% of actual evapotranspiration (mean 2.6%). Therefore, dead storage is a small component of the overall water balance although it is inevitably larger in the Chi and Mun sub-catchments.

3.3. Model validation

Good performance for the validation period is achieved, although it is, in general, inferior to the calibration period (Table 4). NSE for eight stations on the main Mekong is classified as either "excellent" or "very good". Relatively high values of r are achieved for these stations although, with the exception of Mukdahan, they are lower than those of the calibration period. Dv for these stations is generally classed as either "excellent" (upper stations) or "very good" (middle stations) although at Strung Treng (short observed records) and Kratie values are classified as either "excellent" (three PET methods), "very good" (1 method) or "poor" (two methods). Poorer representation of mean flows might relate to the use of unchanging land cover through time, an approach that has been used elsewhere (e.g. Kingston et al., 2011) but which is not completely realistic given the land cover changes which have occurred, especially in the lower part of the catchment. Despite these issues, performance of the six MIKE SHE models for the main Mekong still compares very favourably with previous models of the Mekong (e.g. Hapuarachchi et al., 2008; Västilä et al., 2010; Kingston et al., 2011).

In comparison to the stations on the main Mekong, model performance for the Chi and Mun tributaries is relatively poor, although the short duration of observations (especially for Ubon) should be noted. Results are sensitive to the version of UDel precipitation employed, a finding that was not replicated for the other stations (results for these stations are based on V1.01 for 1991–1996 and V1.02 for 1997–1998). UDel V1.01 leads to a large over estimation of discharge at Yasothon and low NSE and r values (Table 4). The latter are improved by using UDel V1.02 whilst Dv values suggest discharge underestimation (albeit by a smaller amount compared to overestimations for UDel V1.01). Similar differences are evident in results for the Mun. This adds support to the assertion that issues identified during calibration of the models for these stations may lie, at least in part, with the meteorological data for this part of the catchment. As noted above, the use of alternative gridded precipitation datasets such as CRU will be required to assess the impact of this potential source of uncertainty.

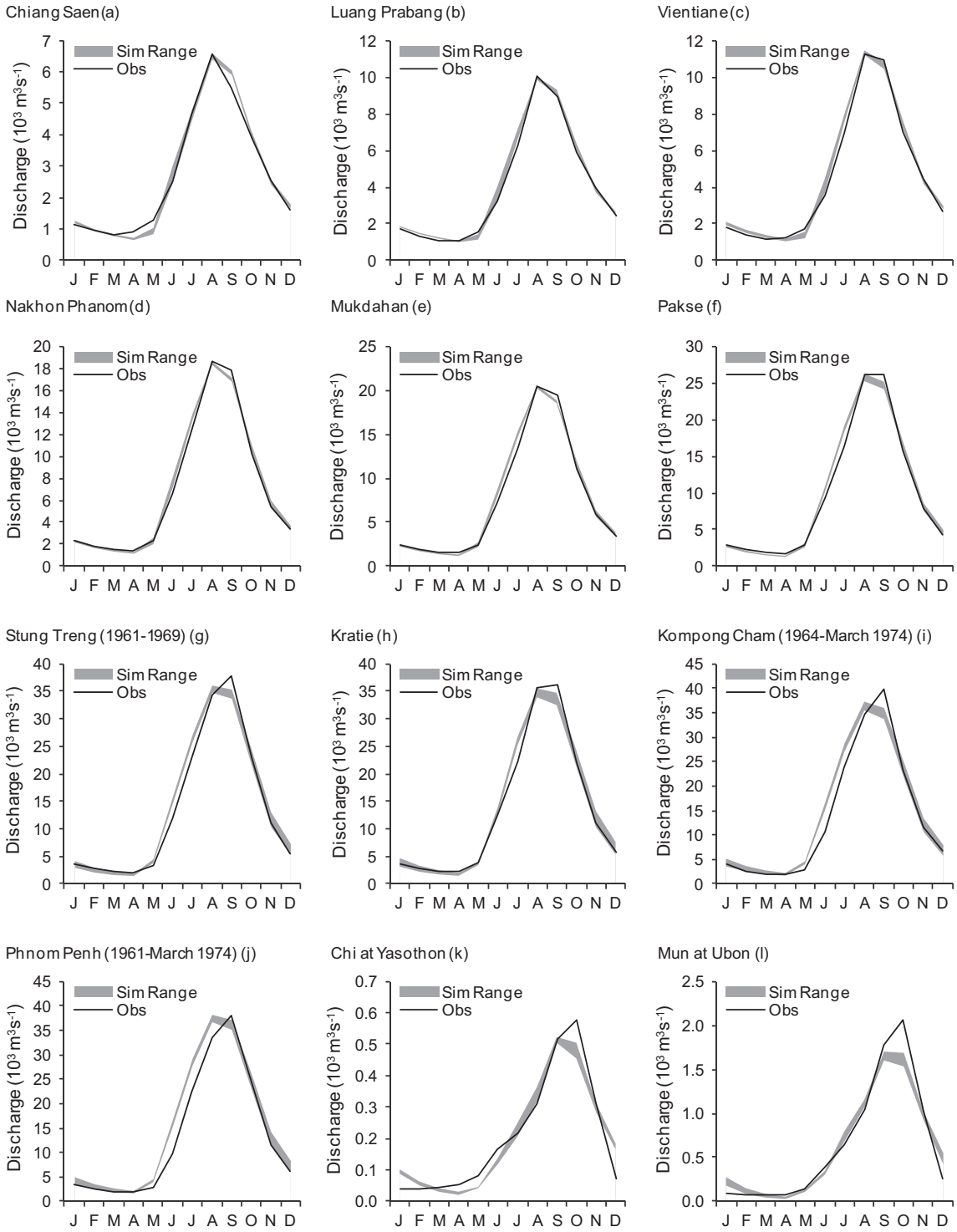

Fig. 3. Observed and range of simulated river regimes from the six MIKE SHE models for all 12 gauging stations within the Mekong catchment for the calibration period (1961–1990 unless indicated otherwise). Letters in brackets refer to the gauging station labels used in Fig. 1.

3.4. Scenario precipitation and temperature

Table 2 provides baseline mean annual total precipitation and mean annual temperature for eight representative sub-catchments as well as changes in each for the seven 2 °C GCM scenarios. CCCMA, MPI and NCAR project increasing annual precipitation for all sub-catchments. The greatest increases occur upstream for CCCMA and NCAR, and downstream for MPI. Annual precipitation declines across all sub-catchments for CSIRO, whilst for IPSL reductions occur across all but three south-central sub-catchments (Chi-Mun, Mekong 2 and Sre Pok). HadCM3 shows increased precipitation over four northern sub-catchments (Lancang to Mekong 1) and decreases elsewhere. HadGEM1 projects increases for the two northernmost sub-catchments (Lancang and Nam Ou) and three southern sub-catchments (Se Kong, Sre Pok, Mekong 3) with declines over the central Mekong. Intra-annual patterns of precipitation change vary. CSIRO, IPSL and MPI exhibit a unimodal response, with increases concentrated around September for CSIRO

Table 4
Range of model performance statistics based on mean monthly discharges from the six MIKE SHE models for twelve gauging stations within the Mekong catchment for the calibration (1961–1990 unless stated otherwise) and validation (1991–1998 unless stated otherwise) periods. Letters after gauging station names refer to the labels used in Fig. 1. Model performance indicators are taken from Henriksen et al. (2008).

Station	Period	Dv (%)[+]		NSE[*]		$r^{\#}$
Chiang Saen (a)	Cal	0.07 to 2.01	☆☆☆☆☆	0.890 to 0.903	☆☆☆☆☆	0.947 to 0.954
	Val (1/91–6/97)	−4.21 to 0.38	☆☆☆☆☆	0.786 to 0.811	☆☆☆☆	0.899 to 0.910
Luang Prabang (b)	Cal	0.77 to 4.08	☆☆☆☆☆	0.894 to 0.911	☆☆☆☆☆	0.948 to 0.956
	Val (1/91–12/97)	−3.58 to 1.59	☆☆☆☆☆	0.835 to 0.863	☆☆☆☆/☆☆☆☆	0.915 to 0.929
Vientiane (c)	Cal	0.23 to 4.77	☆☆☆☆☆	0.902 to 0.918	☆☆☆☆☆	0.951 to 0.956
	Val (1/91–12/96)	−0.44 to 4.83	☆☆☆☆☆	0.891 to 0.908	☆☆☆☆☆	0.946 to 0.956
Nakhon Phanom (d)	Cal	0.21 to 3.67	☆☆☆☆☆	0.906 to 0.919	☆☆☆☆☆	0.952 to 0.957
	Val (1/91–11/95)	−0.52 to 5.63	☆☆☆☆/☆☆☆☆☆	0.892 to 0.910	☆☆☆☆☆	0.949 to 0.954
Mukdahan (e)	Cal	0.94 to 3.96	☆☆☆☆☆	0.903 to 0.914	☆☆☆☆☆	0.951 to 0.957
	Val (1/91–12/95)	−5.39 to 9.50	☆☆☆☆	0.915 to 0.925	☆☆☆☆☆	0.958 to 0.963
Pakse (f)	Cal	−1.89 to 3.75	☆☆☆☆☆	0.896 to 0.910	☆☆☆☆☆	0.949 to 0.955
	Val	−0.56 to 5.86	☆☆☆☆☆/☆☆☆☆	0.893 to 0.907	☆☆☆☆☆	0.947 to 0.955
Stung Treng (g)	Cal (1/61–12/69)	−0.16 to 7.49	☆☆☆☆☆/☆☆☆☆	0.903 to 0.934	☆☆☆☆☆	0.955 to 0.966
	Val (1/91–12/93)	−10.63 to −2.61	☆☆☆/☆☆☆☆☆	0.884 to 0.905	☆☆☆☆☆	0.952 to 0.957
Kratie (h)	Cal	−3.23 to 5.83	☆☆☆☆☆	0.901 to 0.912	☆☆☆☆☆	0.950 to 0.955
	Val	2.19 to 10.16	☆☆☆☆☆/☆☆☆	0.892 to 0.897	☆☆☆☆☆	0.946 to 0.949
Kompong Cham (i)	Cal (1/64–3/74)	1.17 to 9.89	☆☆☆☆☆/☆☆☆☆	0.913 to 0.930	☆☆☆☆☆	0.956 to 0.968
	Val[†]	–		–		–
Phnom Penh (j)	Cal (1/61–3/74)	7.71 to 16.88	☆☆☆☆/☆☆☆	0.888 to 0.905	☆☆☆☆☆	0.953 to 0.963
	Val[†]	–		–		–
Chi at Yasothon (k)	Cal	−0.12 to 1.53	☆☆☆☆☆	0.490 to 0.552	☆☆/☆☆☆	0.712 to 0.743
	Val (1/91–12/95)[‡]	15.65 to 25.26	☆☆☆/☆☆	−0.385 to 0.187	☆	0.408 to 0.552
	Val (1/91–12/95)[•]	−13.74 to −9.78	☆☆☆/☆☆☆☆	0.436 to 0.548	☆☆/☆☆☆	0.676 to 0.753
Mun at Ubon (l)	Cal	−5.00 to 2.91	☆☆☆☆☆	0.537 to 0.613	☆☆☆	0.744 to 0.783
	Val (1/91–12/93)[‡]	−6.09 to 3.49	☆☆☆☆/☆☆☆☆☆	0.117 to 0.381	☆/☆☆	0.532 to 0.648
	Val (1/91–12/93)[•]	−30.63 to −15.79	☆☆/☆☆☆	0.533 to 0.616	☆☆☆	0.755 to 0.799

Performance indicator	Excellent ☆☆☆☆☆	Very good ☆☆☆☆	Fair ☆☆☆	Poor ☆☆	Very poor ☆
Dv	<5%	5–10%	10–20%	20–40%	>40%
NSE	>0.85	0.65–0.85	0.50–0.65	0.20–0.50	<0.20

[+] Percentage deviation in simulated mean flow from observed mean flow (Henriksen et al., 2003).
[*] Nash–Sutcliffe coefficient (Nash and Sutcliffe, 1970).
[#] Pearson correlation coefficient.
[†] Validation not possible due to absence of observations.
[‡] Using UDel V1.01 for 1991–1996, UDel V1.02 for 1997–1998.
[•] Using UDel V1.02 for 1991–1998.

and IPSL (decreases in other months) and May–November for MPI. The other GCMs show a bimodal pattern of change. The greatest increases occur at different times but are concentrated in April–May and September–November.

As discussed above, mean annual temperature is considerably lower over the Lancang and less variable from Mekong 1 downstream. For each GCM, the largest changes (all above 2 °C) occur over the Lancang. Further downstream, increases are closer to the prescribed 2 °C increase. Of the eight sub-catchments in Table 2, the smallest increase in mean temperature is associated with NCAR in five, HadGEM1 in two and CCCMA in one. Increases exceed 2 °C in all sub-catchments for CSIRO. This GCM produces the largest increases for all sub-catchments except Lancang and Mekong 1 (IPSL). The 2 °C threshold is exceeded in all but one sub-catchment (Sre Pok) for MPI and two (Sre Pok and Mekong 3) for IPSL.

3.5. Scenario PET

Table 2 also provides percentage changes in annual PET from the baseline for the eight representative sub-catchments for each PET method and 2 °C GCM scenario. Mean annual PET increases for all sub-catchments for each GCM and PET method (Table 2). Inter-GCM variations in changes in PET are smaller than those for precipitation. On average the mean inter-GCM range of change in annual precipitation for the sub-catchments shown in Table 2 is 14.0% (range: 9.3–18.4%). The corresponding range of mean increases in annual PET varies between 1.4% (1.2–2.1%) for BC PET and 5.9% (4.2–10.0%) for PN PET.

Of the 42 combinations of GCMs and PET methods (seven GCMs × six PET methods), the largest increases in mean annual PET occur over the Lancang in 33 cases (78.6%) including the largest increases in PET for the BC, HM, HS and PT methods across all GCMs. Increases in PET for BC, HS and PT for the more southerly sub-catchments are relatively consistent and notably lower than those for the Lancang.

Across GCMs, there is some consistency in the relative order of magnitude of increase due to different PET methods. Of the 56 sub-catchment/GCM combinations in Table 2 (eight sub-catchments × seven GCMs), BC produces the smallest increases in mean annual PET in 31 (55.4%) followed by HS (22 instances or 39.3%). Combined, these two methods therefore account for 53 (94.6%) of the smallest increases. For the second lowest changes, the relative order is approximately reversed, with HS accounting for 30 (53.6%) and BC 19 (33.9%) sub-catchment/GCM combinations. LN is associated with most of the largest PET increases (46 or 82.1%), followed by HM (10 or 17.9%). HM and LN also account for all of the second highest increases, with the relative order being exactly reversed to that of the highest.

There are also consistencies in the order of magnitude of increases in mean annual PET due to different GCMs. Of the 48 sub-catchment/PET method combinations (eight sub-catchments × six PET methods), the smallest increases are associated with NCAR in 36 (75.0%). The majority of the remaining smallest increases (8 or 16.7% of the 48 combinations) are due to HadGEM1. The largest PET increases are predominantly associated with CSIRO (23 or 47.9%) and HadCM3 (18 or 37.5%). CSIRO, associated with

the largest changes in mean temperature in most sub-catchments, also simulates the greatest number of second largest PET increases (22 or 45.8%) followed by IPSL (13 or 27.1%) and HadCM3 (10 or 20.8%).

The dominant seasonal distributions of PET through the year do not change from those of the baseline period (Fig. 2). Monthly changes do, however, demonstrate some consistent patterns for different PET methods and GCMs. This is exemplified in Fig. 4, which presents percentage changes in mean monthly PET for the Mekong 1 sub-catchment (selected due to its large size and central position). The four temperature-based methods (BC, HM, HS and LN) show very similar temporal changes for a given GCM, albeit

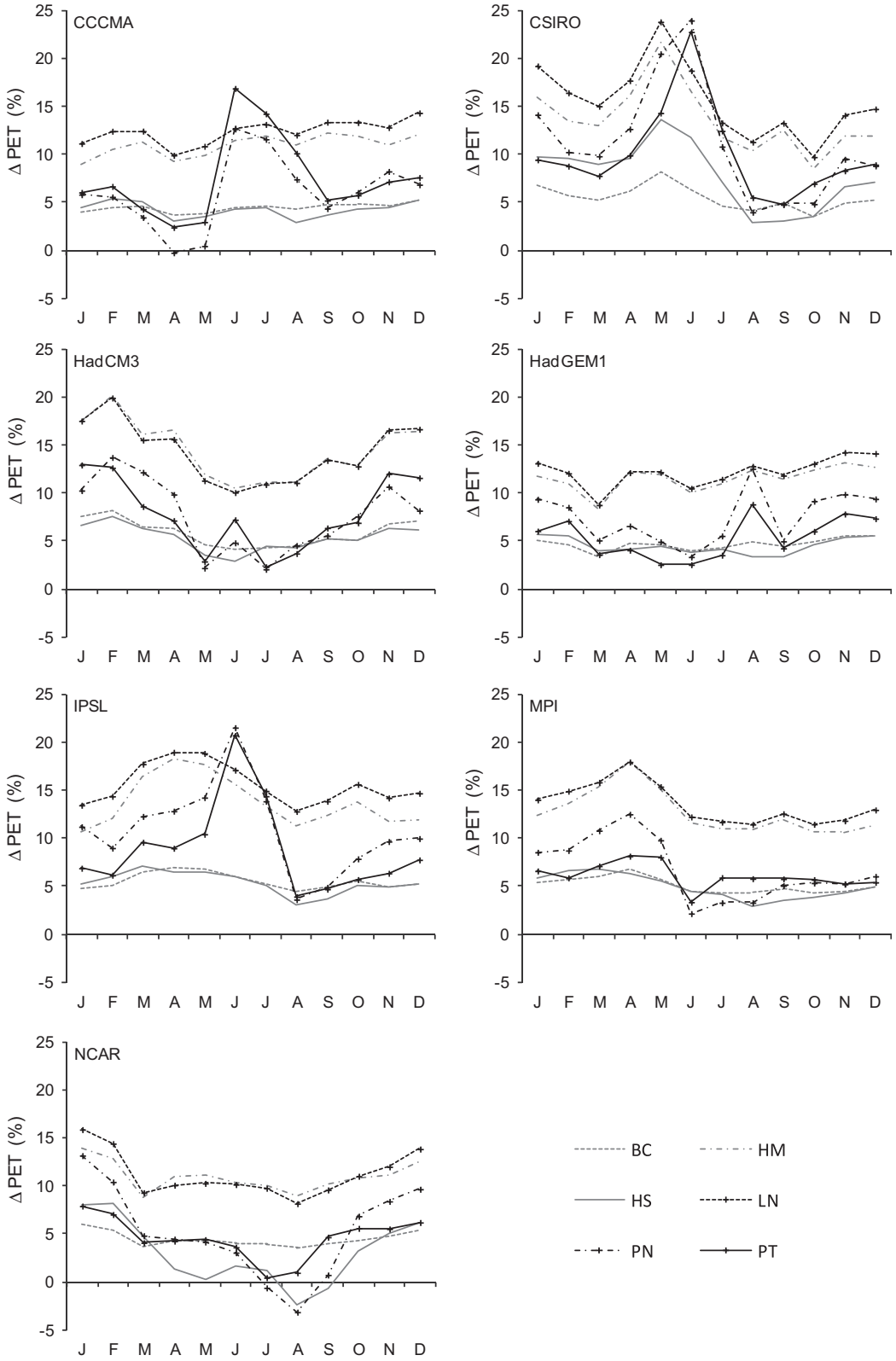

Fig. 4. Mean monthly change (%) in PET from the baseline for the Mekong 1 sub-catchment (sub-catchment 4 in Fig. 1) for each PET method and GCM.

with different magnitudes. Changes for BC and HS are lower than those for HM and LN (which produce the largest increases in mean annual PET). Changes in monthly PET for these methods for a particular GCM reflect the corresponding changes in temperature. For CCCMA and HadGEM1, changes in temperature and hence PET are characterised by the lowest intra-annual variability. The smallest gains are in March or April and they increase gradually through summer and, in particular, autumn/early winter. In contrast, CSIRO, ISPL and MPI demonstrate peak changes during the period March–May (most clearly demonstrated for CSIRO with a large change in January not repeated for the other GCMs). The smallest changes in PET occur in July–October after which they then increase. BC, HM, HS and LN PET for HadCM3 and NCAR are characterised by relatively large changes between November and February and smaller increases in the middle of the year (HS PET declines below the baseline in August for NCAR).

Changes in mean monthly PET for the two remaining methods (PN and PT – which include variables other than temperature) follow those of the temperature-based methods for much of the year. However, there are some notable differences. The largest changes are associated with a distinct June peak that, for CCCMA and IPSL, extends into July (August for CCCMA). A much smaller peak is also evident in June for PN and PT for the HadCM3 GCM, whilst the largest changes in PET for both methods for HadGEM1 is due to a similar peak in August.

3.6. Scenario river discharge

Table 5 presents mean baseline discharge and percentage changes in these discharges for the six models employing different PET methods for each GCM scenario. Results are provided for eight representative gauging stations. The variability in mean baseline and scenario discharges is expressed as the difference between the largest and smallest mean discharge for a given scenario (i.e. the range) as a percentage of the overall average of the mean discharges for that scenario. Changes in mean discharge for each PET method/2 °C GCM scenario are also shown in Fig. 5 for six representative gauging stations.

The range of simulated mean discharges at each gauging stations increases for all GCMs for each PET method compared to the baseline (Table 5). For the baseline, the difference between the largest and smallest mean discharges is, on average, 5.6% of the overall mean from the six models. The mean inter-MIKE SHE model range in mean discharge increases to between 9.2% (NCAR) and 11.9% (IPSL) for the GCM scenarios. However, uncertainty associated with different GCMs is substantially greater than that due to alternative PET methods. The largest range of change in mean discharge for any gauging station on the main Mekong due to the different GCMs simulated by one of the MIKE SHE models is 37.9% (Chiang Saen, PN PET, −18.0% and +19.9% for IPSL and HadCM3, respectively). This is slightly exceeded by the 40.8% range for Ubon (BC PET, HadGEM1: −14.6%, MPI: 26.1%). The average inter-GCM range of change in mean discharge for the eight gauging stations in Table 5 simulated by the MIKE SHE models is 29.4% (29.5% for all 12 stations). In contrast, the largest range of change in mean discharge for any gauging station (Chiang Saen) simulated for any GCM (HadCM3) by the different MIKE SHE models is 15.4% (HM:+4.5%, PN:+19.9%). The average inter-MIKE SHE model range of change for mean annual discharge for the eight gauging stations for the seven scenarios is 8.3% (8.4% for all 12 gauging stations).

For some scenarios direction of change in mean discharge is consistent irrespective of PET method. All models simulate catchment-wide increases in mean discharge for CCCMA and NCAR. The magnitudes of increases broadly concur with the relative magnitude of changes in PET. The HM and LN models (largest PET increases) produce the smallest increases in discharge at most gauging stations. Conversely, the BC and HS models (smallest increases in PET), project the largest increases in mean discharge. For CCCMA, the largest increases at seven stations are due to BC PET (the other PN PET), whilst for NCAR, HS PET produces the largest increases at six stations (BC and PN each accounting for one of the remaining stations).

The same spatial patterns of change along the main Mekong are evident for the different PET methods for both CCCMA and NCAR. For CCCMA the magnitudes of the increases in mean discharge rise as far as Pakse and then decline due to the smaller gains in precipitation in the lower Mekong. Similarly for NCAR, discharge increases rise towards Vientiane or Mukdahan and then decline further downstream. In many cases NCAR produces the largest increases in mean discharge along the main Mekong. Conversely, increases in the mean discharge of the Mun at Ubon (and for the Chi at Yasothon) are consistently larger for CCCMA compared to NCAR due to the larger increases in precipitation over this sub-catchment for CCCMA.

Mean discharge declines at every gauging station for the CSIRO GCM for all six MIKE SHE models (Table 5). In all cases, the magnitude of the declines decreases in a downstream direction. The largest reductions at four stations in Table 5 are due to HM PET, with LN PET accounting for the second largest reductions at these stations. This order is reversed for the other four stations. The BC PET MIKE SHE model projects the smallest declines in discharge at six stations, with HS PET accounting for the other two. The latter PET method is responsible for the second smallest declines in discharge at five stations, the remaining three resulting from either BC (two stations) or PN PET (one station).

For the remaining four GCMs, some uncertainty in the direction of change in mean discharge is introduced by PET method. For IPSL, mean discharge generally declines under climate change at all gauging stations on the main Mekong, for all PET methods. The magnitude of these declines reduces downstream. However, whilst for HM and LN discharge also declines for the Mun at Ubon (repeated for the Chi at Yasothon), the other models employing alternative PET methods project relatively small increases (Table 5, Fig. 5). LN and HM are associated with the largest increases in annual PET for the Mun (14.2% and 12.4%, respectively – Table 2). In contrast, changes in annual PET for the other methods are lower (maximum 9.1% for PN). Although the Mun experiences an overall small (0.1%) decline in annual precipitation, increases during the wet season coupled with smaller increases in PET for these four methods account for the modest increases in mean discharge.

Some uncertainty due to PET method is evident for MPI. Annual precipitation increases in all sub-catchments, although increases are relatively small, especially upstream (e.g. the Lancang). Conversely, increases in the original LN PET are larger than those for CCCMA and NCAR, the other scenarios with catchment-wide increases in precipitation. Mean discharge therefore declines in the upper Mekong until Luang Prabang and then increases. In contrast, for BC and HS mean discharge increases at all gauging stations. These two PET methods result in the smallest increases in annual PET for MPI. The relatively modest increases in precipitation are therefore not offset by increased evapotranspiration. Increases in annual PN PET are slightly larger than those for BC and HS (Table 2) so that very small (<1%) declines in mean discharge are restricted to Chiang Saen. The larger PET increases for HM and PT cause declines in Mekong discharge to extend downstream to Vientiane.

For HadCM3 and the LN PET model, mean discharge increases in the upper Mekong as far as Pakse. These increases decline downstream whilst below Pakse discharges decline, albeit by small amounts (Table 5). This pattern was attributed to the relatively large (10.1%, Table 2) increases in precipitation over the Lancang and smaller increases over Mekong 1 that offset elevated evapotranspiration (Thompson et al., 2013a). Further south, precipitation

Table 5
Mean baseline discharge ($m^3 s^{-1}$) and change from baseline mean discharge (%) for the different PET methods for each GCM at eight gauging stations within the Mekong catchment. Letters in brackets refer to the gauging station labels used in Fig. 1. Italicised values indicate negative changes compared to the baseline. The range of mean discharges for the baseline and each GCM from the different PET methods are also indicated (% of overall mean discharge from the PET methods for that scenario).

Scenario	PET/ Scenario	Chiang Saen (a)	Luang Prabang (b)	Vientiane (c)	Mukdahan (e)	Pakse (f)	Kratie (h)	Phnom Penh (j)	Ubon (l)
Baseline ($m^3 s^{-1}$)	BC	2755.4	4115.9	4698.1	7813.0	9804.1	12931.2	13304.4	635.9
	HM	2752.6	4108.1	4701.2	7871.5	9986.2	13411.8	13813.3	651.7
	HS	2705.5	3995.3	4515.0	7780.2	10058.0	13867.1	14336.8	636.3
	LN	2724.9	4115.2	4719.5	7643.0	9604.8	13000.5	13428.8	601.4
	PN	2702.6	3998.0	4599.1	7745.0	10086.5	13964.0	14437.6	633.8
	PT	2702.5	4126.4	4677.4	7785.3	10164.0	14141.5	14620.2	618.5
CCCMA (% change)	BC	11.6	12.6	13.4	14.0	15.3	13.4	13.3	22.0
	HM	4.2	4.8	5.6	7.5	8.6	7.0	6.9	12.5
	HS	10.7	11.9	13.1	13.6	14.5	12.3	12.2	19.4
	LN	7.1	6.8	7.3	8.2	8.9	7.1	7.0	11.2
	PN	11.9	12.2	12.4	12.5	12.9	10.9	10.8	13.8
	PT	5.2	6.2	6.9	8.7	9.5	7.9	7.9	11.7
CSIRO (% change)	BC	*−17.0*	*−16.2*	*−15.3*	*−12.0*	*−10.6*	*−9.1*	*−8.9*	*−2.9*
	HM	*−24.0*	*−23.9*	*−22.8*	*−18.3*	*−16.8*	*−14.7*	*−14.4*	*−10.1*
	HS	*−18.3*	*−17.5*	*−16.8*	*−12.8*	*−10.9*	*−9.1*	*−8.8*	*−1.4*
	LN	*−21.3*	*−21.7*	*−21.2*	*−18.0*	*−16.9*	*−15.0*	*−14.7*	*−11.7*
	PN	*−17.9*	*−17.9*	*−16.9*	*−13.7*	*−12.1*	*−10.1*	*−9.8*	*−3.9*
	PT	*−20.3*	*−19.6*	*−18.5*	*−14.8*	*−13.0*	*−11.0*	*−10.7*	*−5.2*
HadCM3 (% change)	BC	14.5	14.7	12.9	8.4	6.6	3.7	3.3	*−0.5*
	HM	4.5	4.8	3.4	0.9	*−0.8*	*−3.1*	*−3.5*	*−8.8*
	HS	13.3	14.1	12.7	8.2	6.2	3.0	2.6	*−1.4*
	LN	11.3	9.9	7.8	3.7	1.5	*−1.7*	*−2.1*	*−8.4*
	PN	19.9	19.8	17.4	11.1	8.3	4.5	4.1	*−2.3*
	PT	10.2	11.0	9.8	6.4	4.7	1.8	1.5	*−2.4*
HadGEM1 (% change)	BC	3.2	1.1	*−0.6*	*−3.8*	*−5.6*	*−4.4*	*−4.4*	*−14.6*
	HM	*−4.4*	*−6.3*	*−7.7*	*−9.5*	*−11.1*	*−9.4*	*−9.4*	*−20.5*
	HS	2.4	1.1	*−0.4*	*−3.2*	*−4.6*	*−3.1*	*−3.0*	*−12.2*
	LN	0.2	*−3.6*	*−5.6*	*−8.6*	*−10.7*	*−9.3*	*−9.2*	*−21.0*
	PN	1.3	*−0.1*	*−1.4*	*−4.2*	*−5.8*	*−4.3*	*−4.3*	*−14.1*
	PT	1.1	0.0	*−1.0*	*−3.5*	*−5.0*	*−3.6*	*−3.5*	*−14.0*
IPSL (% change)	BC	*−16.0*	*−13.3*	*−11.5*	*−7.2*	*−4.8*	*−3.8*	*−3.8*	6.8
	HM	*−24.6*	*−22.6*	*−20.5*	*−14.5*	*−12.0*	*−10.2*	*−10.1*	*−1.5*
	HS	*−15.8*	*−13.1*	*−11.4*	*−6.6*	*−4.3*	*−3.2*	*−3.1*	5.7
	LN	*−19.9*	*−18.3*	*−16.9*	*−12.9*	*−11.0*	*−9.7*	*−9.7*	*−2.8*
	PN	*−18.0*	*−16.1*	*−14.3*	*−9.6*	*−7.5*	*−5.6*	*−5.5*	0.8
	PT	*−20.0*	*−17.5*	*−15.7*	*−10.5*	*−8.2*	*−6.3*	*−6.2*	0.3
MPI (% change)	BC	1.1	3.7	5.3	7.6	10.5	11.2	11.5	26.1
	HM	*−7.9*	*−5.9*	*−4.2*	0.1	2.9	4.3	4.7	16.8
	HS	0.3	3.0	4.7	7.3	9.8	10.5	10.9	23.1
	LN	*−2.4*	*−1.0*	0.1	2.5	4.8	5.6	5.9	16.9
	PN	*−0.9*	1.7	3.2	6.1	8.7	10.0	10.4	21.7
	PT	*−5.4*	*−2.1*	*−0.5*	3.7	6.5	8.0	8.5	19.7
NCAR (% change)	BC	10.9	15.5	16.1	16.2	15.3	12.5	12.3	9.5
	HM	2.2	6.2	7.0	9.0	8.3	6.1	6.0	2.4
	HS	12.4	17.6	18.5	17.9	16.4	13.2	13.0	9.0
	LN	8.7	12.4	12.6	12.7	11.4	8.2	8.1	3.2
	PN	12.8	17.4	17.3	16.9	15.3	12.1	12.0	7.1
	PT	8.9	13.5	13.8	14.3	13.0	10.1	9.9	5.4
Range of mean discharges (% of overall mean from the six PET methods)	Baseline	1.9	3.2	4.4	2.9	5.6	8.9	9.4	8.0
	CCCMA	7.8	7.4	7.1	7.4	9.5	11.1	11.2	14.8
	CSIRO	8.9	9.8	9.2	9.1	11.4	13.0	13.1	16.3
	HadCM3	11.9	10.6	10.4	8.1	11.3	13.2	13.3	13.5
	HadGEM1	7.7	7.7	7.3	7.5	11.6	14.4	14.5	15.9
	IPSL	10.8	11.4	10.7	8.7	11.8	13.3	13.5	14.8
	MPI	9.5	10.0	9.4	7.1	9.1	11.1	11.3	13.0
	NCAR	8.1	8.5	8.0	6.7	9.0	10.8	11.0	11.3

declines so that, in combination with higher PET, discharges decrease. The larger increases in HM PET, especially over upstream sub-catchments, cause the point at which mean discharge declines to shift upstream to between Mukdahan and Pakse (Table 5). In contrast, the consistently smaller increases in PET for BC, HS, PN and PT (all $\leqslant$ 10%, Table 2) cause the influence of enhanced upstream precipitation to extend throughout the catchment. Mean discharges increase along the main Mekong, although the magnitude of changes declines in a downstream direction. The particularly small increase in PN PET over the Lancang results in the largest discharge increases. The influence of declining precipitation in the south combined with higher PET is indicated by declines in

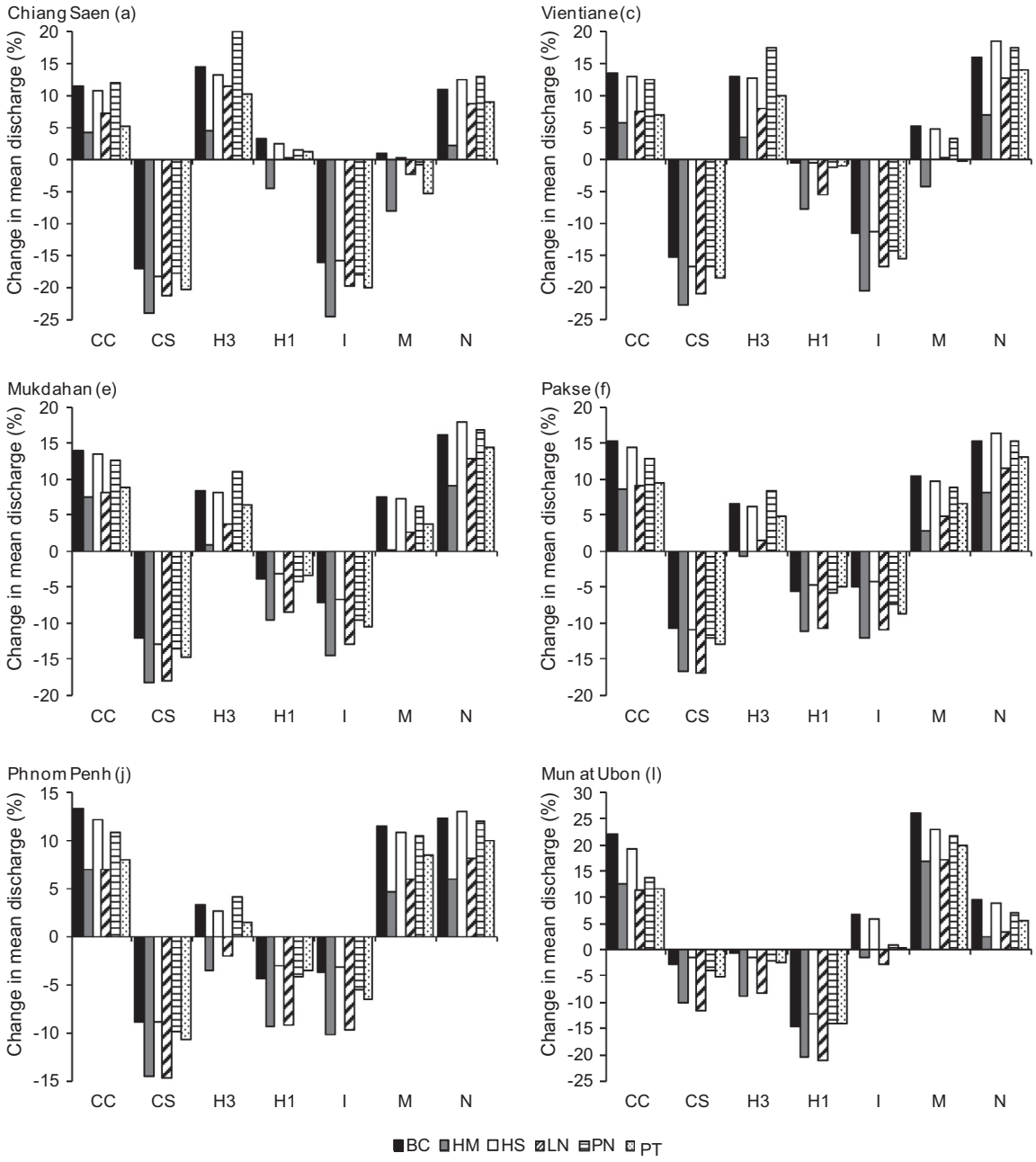

Fig. 5. Change from baseline mean discharge for the 2 °C, seven GCM scenarios and each PET method for six gauging stations within the Mekong catchment. Letters in brackets refer to the gauging station labels used in Fig. 1. CC: CCCMA; CS: CSIRO; H3: HadCM3; H1: HadGEM1; I: IPSL; M: MPI; N: NCAR.

Mun discharge at Ubon. The largest reductions are due to HM and LN (larger PET increases) and the smallest from BC (smallest increase in PET).

A similar pattern to HadCM3 is evident for HadGEM1, although the point at which increases in mean discharge switch to declines is further upstream since enhanced precipitation in the upper Mekong is restricted to the two northernmost sub-catchments. For LN and PN increasing mean discharge is limited to Chiang Saen, after which discharge declines until Pakse. Modest increases in precipitation over southerly sub-catchments limit further reductions at the lowest gauging stations. Larger increases in HM PET over the Lancang (16.1% compared to 12.4% for LN PET, Table 2) offset increases in precipitation, so that mean discharge at Chiang Saen declines. In contrast, smaller PET increases for the remaining methods cause increases in discharge to extend downstream to Luang Prabang (no change for PT). For all PET methods, the largest declines in discharge on the main Mekong are at Pakse. Impacts of elevated PET and lower precipitation is clearly demonstrated for the Mun at Ubon. The largest reductions in discharge result from HM and LN and the smallest from HS PET.

As an alternative way to compare PET uncertainty between methods and GCMs, changes in areal PET were considered (Fig. 6). These were derived by weighting PET changes for each sub-catchment by the proportion these sub-catchments comprise of the total area draining to a gauging station. Areal PET for Chiang Saen and Ubon therefore correspond to changes for the Lancang and Mun sub-catchments, respectively whilst those for Phnom Penh are based on changes over 11 upstream sub-catchments. Fig. 6 demonstrates the strong, but not perfect, negative relationship between increase in PET and increase in discharge, as well

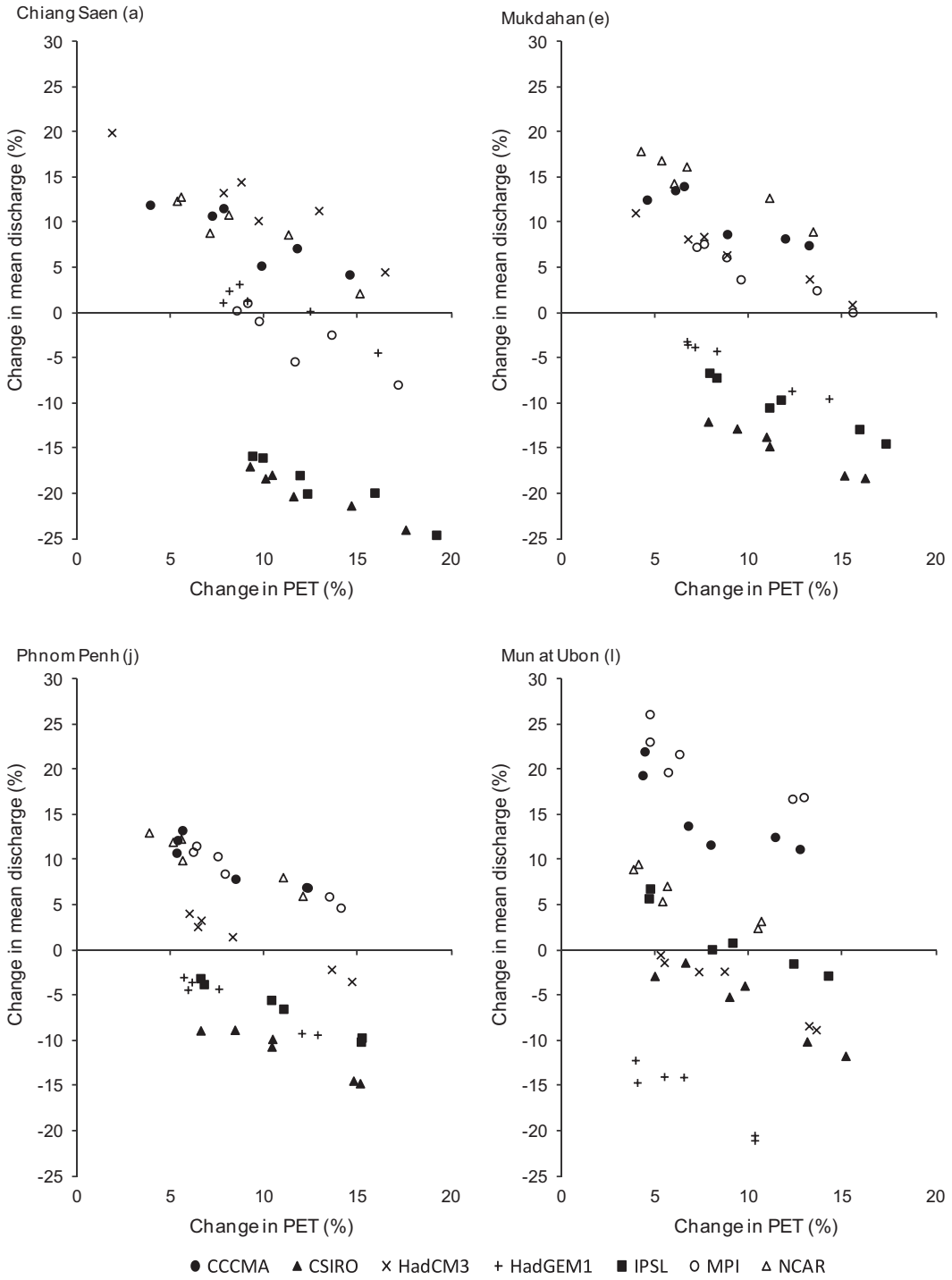

Fig. 6. Relationship between change in mean discharge and change in weighted mean PET for each GCM and PET method for four gauging stations within the Mekong catchment. Letters in brackets refer to the gauging station labels used in Fig. 1.

as PET method-related uncertainty in the direction of discharge change at some gauging stations for some GCMs (Chiang Saen: HadGEM1 and MPI; Phnom Penh: HadCM3; Ubon: IPSL). Greater GCM-related uncertainty is indicated by the wider range of change in mean discharge for the seven GCMs compared to those due to the different PET methods.

At a monthly resolution, greater GCM-related uncertainty compared to that associated with PET methods is evident (Fig. 7). For a given GCM, mean monthly discharges simulated by the different models are broadly similar and follow the patterns described by Thompson et al. (2013a). For example, for CSIRO all six models simulate declines in the rising limb of the seasonal peak, especially further upstream. Peak discharges are delayed from August for the baseline to September. Similarly, all six models simulate this delayed peak for NCAR but with the magnitude of the peak increasing.

The range of scenario mean monthly discharges is greater than that for the baseline. This is most apparent during the seasonal peak, although the range increases in most months. For all 12 gauging stations, the baseline inter-MIKE SHE model range in August and September discharges, expressed as a percentage of the overall mean from the six models for the respective month, is on

average 4.4% and 4.5%, respectively. In contrast, for the 2 °C GCM scenarios these ranges vary between 7.3% (MPI) and 12.5% (HadGEM1) for August and between 8.0% (NCAR) and 10.7% (HadCM3) for September. The greatest individual change in the range of peak discharges occurs at Chiang Saen for HadCM3. Mean baseline August discharge at this station ranges between 6385.8×10^3 m^3 s^{-1} (HS) and 6582.4×10^3 m^3 s^{-1} (PN) (range: 196.6×10^3 m^3 s^{-1} or 3.0% of the mean from the six models). This compares to a range of 916.1×10^3 m^3 s^{-1} (13.9% of the six model mean) for HadCM3. Results for individual models range between a 4.3% decrease (HM PET) to an increase of 8.0% (PN PET).

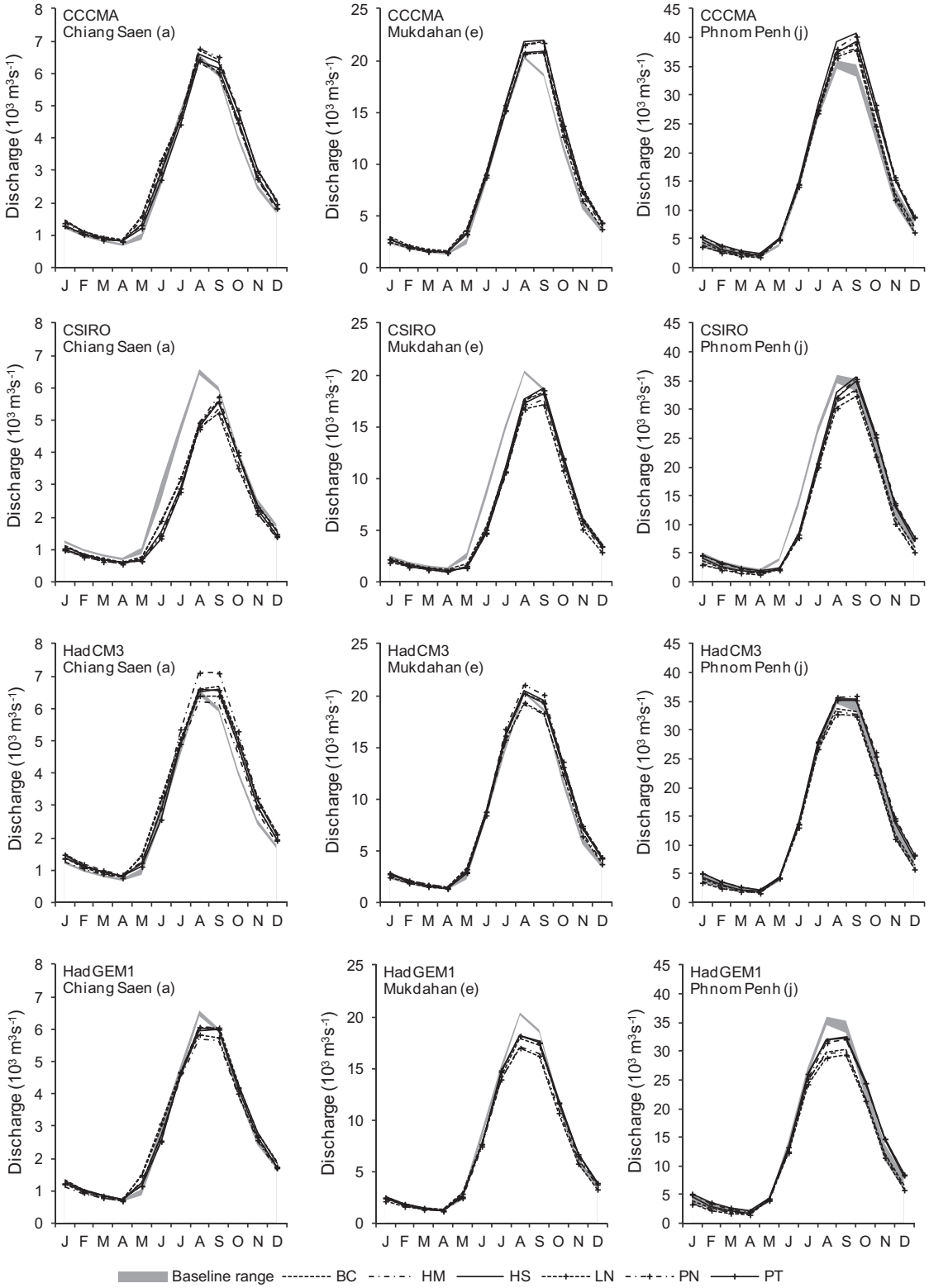

Fig. 7. River regimes for the baseline and 2 °C, seven GCM climate change scenarios and each PET method for three gauging stations within the Mekong catchment. Letters in brackets refer to the gauging station labels used in Fig. 1.

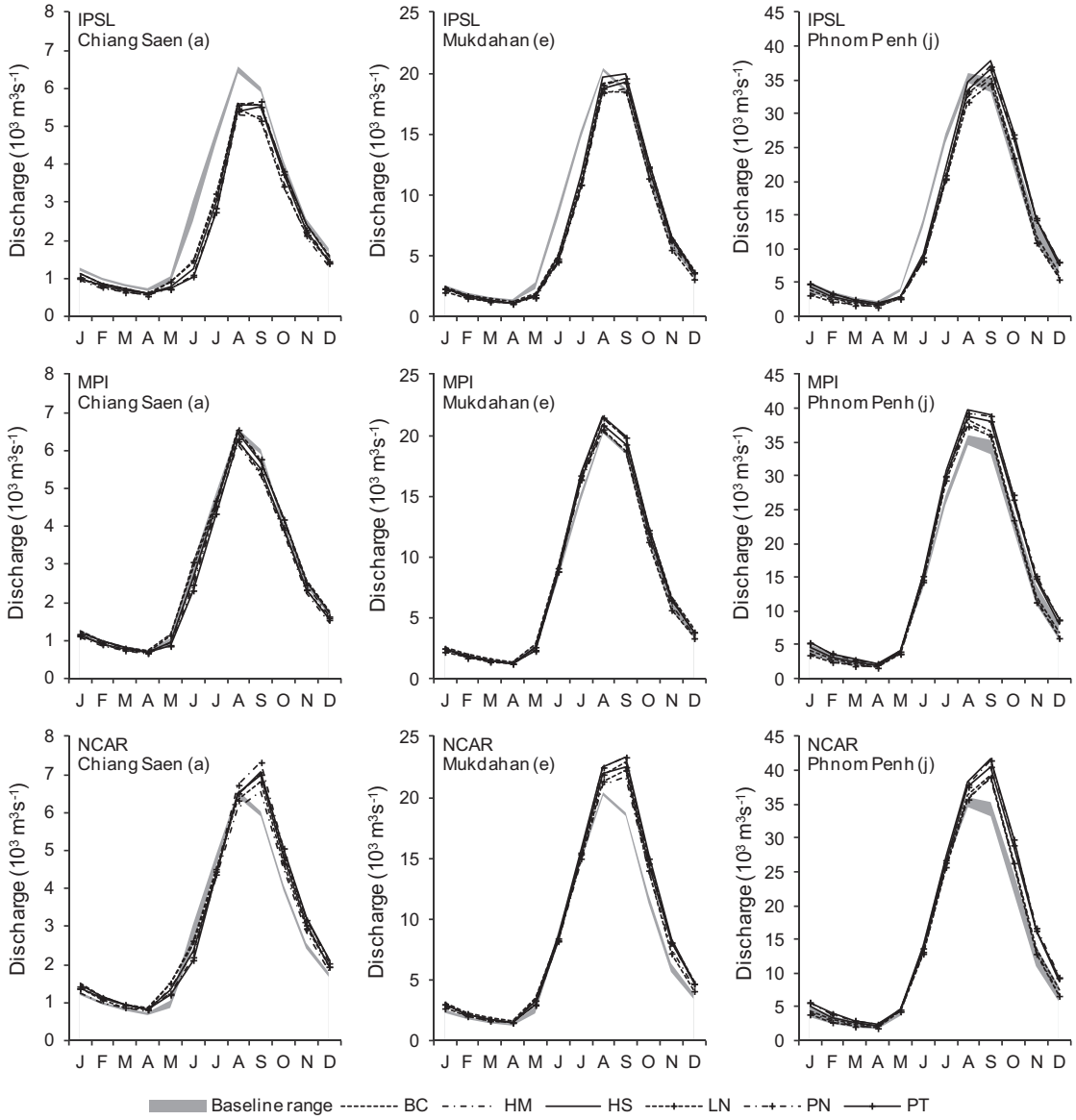

Fig. 7 (*continued*)

Uncertainty in the direction of change in either high or low flows, and in some cases both, is introduced for all scenarios due to the different PET methods (Table 6). For some GCMs, uncertainty is only associated with either high or low flows and is restricted to parts of the catchment. Both Q5 and Q95 (discharges equalled or exceeded for 5% and 95% of the time, respectively) increase throughout the main Mekong for NCAR. The smallest increases are due to HM and the largest predominantly associated with HS or PN PET. Although Q5 increases for Ubon, half of the models project declines in Q95. Conversely, for CSIRO Q5 and Q95 decline for the main Mekong for all models (largest Q5 and Q95 decreases due to LN and HM, respectively). Q95 also consistently declines at Ubon, but Q5 increases for all the models except those employing HM and LN PET. Uncertainty in the direction of change of high flows for CCCMA is restricted to the top of the catchment. HM, LN and PT project declines in Q5, albeit of small magnitude, that are contrary to increases simulated throughout the Mekong by the other models. All six models, however, project increasing low flows. The largest upstream increases in Q95 are from BC PET whilst further downstream either HS or PN PET generate the largest changes. Most of the smallest increases are due to PT PET.

HadGEM1 and IPSL show consistent declines in either high (HadGEM1, except for a negligible change at Vientiane for BC PET) or low (ISPL) flows, with some consistency in the relative magnitude of these changes due to the different PET methods. Conversely, uncertainty in low and high flows, respectively is projected for these two GCMs at the majority of stations. For HadGEM1, HM projects declines in Q95 throughout the Mekong. Whilst HS projects increases in low flows along most of the main Mekong, the other models project increases at upstream stations and declines further downstream (a modest increase at Phnom Penh for PN). Although all models show declines in Q5 for ISPL as far as Vientiane, there is uncertainty further downstream. The HS model projects increasing high flows from Mukdahan, whilst the HM and LN models show declines in Q5 along the length of the main Mekong.

Direction of change in Q95 for HadCM3 is consistent between MIKE SHE models - increases on the main Mekong and declines for the Mun and Chi. However, HM and LN project declines in high flows, which grow in magnitude from Nakhon Phanom downstream. The other models project increases in Q5 that tend to decline in a downstream direction. HM also shows declines in Q5 in the upper catchment (Chiang Saen and Luang Prabang) that are

Table 6
Changes in Q5 and Q95 discharge (%) for the different PET methods for each GCM at six gauging stations within the Mekong catchment (CS: Chiang Saen; Vi: Vientiane; Mu: Mukdahan; Pa: Pakse; PP: Phnom Penh; Ub: Ubon. Letters in brackets refer to the gauging station labels used in Fig. 1. Italicised values indicate negative changes compared to the baseline).

		Q5						Q95					
GCM	PET	CS (a)	Vi (c)	Mu (e)	Pa (f)	PP (j)	Ub (l)	CS (a)	Vi (c)	Mu (e)	Pa (f)	PP (j)	Ub (l)
CCCMA	BC	4.7	8.0	12.8	15.0	13.2	21.9	21.3	19.4	19.2	22.8	18.2	24.0
	HM	*−3.0*	*−0.2*	7.4	9.8	7.7	15.4	8.9	8.9	13.0	13.4	8.5	15.6
	HS	3.2	4.9	11.9	13.8	12.7	19.7	15.9	18.8	23.2	23.9	18.4	29.0
	LN	0.0	*−2.2*	7.4	11.3	8.3	15.0	14.0	13.7	15.8	14.9	11.9	21.2
	PN	4.6	2.9	10.7	12.3	12.0	14.5	18.0	15.5	17.4	19.3	12.7	25.6
	PT	*−1.2*	*−0.8*	8.9	10.3	10.1	12.8	8.5	8.0	9.8	12.2	8.3	16.8
CSIRO	BC	*−12.8*	*−8.6*	*−8.1*	*−6.7*	*−6.2*	4.2	*−14.9*	*−13.9*	*−12.5*	*−11.1*	*−11.0*	*−8.3*
	HM	*−16.2*	*−14.6*	*−10.1*	*−9.8*	*−8.5*	*−0.6*	*−22.6*	*−25.0*	*−18.9*	*−19.0*	*−19.2*	*−14.5*
	HS	*−12.9*	*−10.5*	*−6.3*	*−5.6*	*−5.4*	6.4	*−17.7*	*−20.0*	*−13.9*	*−12.3*	*−11.5*	*−10.3*
	LN	*−17.2*	*−16.9*	*−13.9*	*−13.2*	*−10.7*	*−5.7*	*−21.5*	*−22.6*	*−19.6*	*−17.9*	*−17.6*	*−10.8*
	PN	*−9.7*	*−12.2*	*−7.2*	*−7.1*	*−5.6*	6.6	*−16.7*	*−19.6*	*−15.9*	*−14.5*	*−13.1*	*−15.3*
	PT	*−10.8*	*−11.7*	*−8.7*	*−8.0*	*−6.2*	3.9	*−18.7*	*−21.3*	*−18.7*	*−16.4*	*−13.8*	*−26.3*
HadCM3	BC	10.3	9.3	2.7	3.1	*−0.1*	0.9	20.6	15.6	14.6	16.0	9.6	*−4.5*
	HM	*−0.6*	2.6	*−2.5*	*−3.0*	*−4.1*	*−8.5*	7.1	4.6	6.0	3.8	0.0	*−9.9*
	HS	6.5	7.3	2.1	3.0	0.9	*−2.5*	18.3	17.4	16.2	17.1	8.3	*−3.7*
	LN	8.2	3.2	*−2.2*	*−1.9*	*−4.5*	*−7.2*	15.6	11.0	10.3	9.0	3.3	*−4.9*
	PN	14.6	9.6	3.8	5.5	3.6	*−2.0*	28.2	22.1	20.4	18.2	9.4	*−4.9*
	PT	7.0	4.3	0.6	2.9	2.2	*−2.5*	15.8	12.4	10.7	10.0	4.4	*−12.5*
HadGEM1	BC	*−0.1*	0.0	*−7.3*	*−10.3*	*−10.5*	*−8.9*	7.0	1.4	*−1.9*	*−0.4*	*−0.7*	*−12.3*
	HM	*−7.1*	*−7.1*	*−11.5*	*−13.7*	*−13.8*	*−14.9*	*−4.9*	*−6.5*	*−7.1*	*−9.1*	*−8.6*	*−19.1*
	HS	*−2.1*	*−2.0*	*−5.7*	*−8.3*	*−9.7*	*−9.3*	3.1	*−0.3*	0.5	1.4	0.3	*−10.6*
	LN	*−3.5*	*−8.3*	*−12.4*	*−15.4*	*−15.3*	*−12.8*	1.7	*−6.0*	*−4.9*	*−3.7*	*−5.7*	*−19.0*
	PN	*−1.0*	*−5.7*	*−9.0*	*−9.8*	*−10.0*	*−11.3*	1.8	*−0.2*	*−2.1*	*−3.1*	*−1.7*	*−14.6*
	PT	*−2.2*	*−4.1*	*−6.9*	*−8.8*	*−9.0*	*−12.0*	2.0	0.1	−1.8	−2.7	0.2	*−22.8*
IPSL	BC	*−6.2*	*−2.6*	*−1.7*	2.3	2.2	13.0	*−14.9*	*−10.8*	*−11.8*	*−9.3*	*−8.6*	*−0.1*
	HM	*−11.7*	*−7.9*	*−4.5*	*−1.8*	*−1.2*	7.0	*−27.9*	*−20.9*	*−19.8*	*−18.6*	*−18.4*	*−7.9*
	HS	*−6.4*	*−0.9*	0.3	2.8	4.6	14.3	*−17.4*	*−15.3*	*−10.9*	*−8.9*	*−5.7*	*−3.3*
	LN	*−11.6*	*−11.4*	*−7.0*	*−1.4*	*−3.4*	5.3	*−19.5*	*−16.9*	*−17.4*	*−17.1*	*−15.5*	*−4.0*
	PN	*−7.1*	*−6.1*	*−4.1*	*−0.0*	0.8	11.9	*−19.4*	*−17.4*	*−14.5*	*−12.8*	*−9.0*	*−10.8*
	PT	*−9.2*	*−7.5*	*−4.5*	*−1.1*	1.2	9.2	*−20.7*	*−19.3*	*−17.6*	*−14.7*	*−9.8*	*−17.6*
MPI	BC	2.5	7.6	6.4	8.6	9.9	24.5	*−0.1*	3.5	4.1	4.9	7.9	14.9
	HM	*−4.7*	0.0	2.7	3.0	5.3	15.1	*−9.8*	*−7.5*	*−4.1*	*−4.5*	*−3.0*	5.6
	HS	1.7	4.8	6.2	8.5	9.6	19.8	*−0.6*	4.9	6.1	7.4	9.4	15.5
	LN	*−1.4*	*−0.9*	2.1	4.7	6.2	16.2	*−1.2*	*−1.8*	*−4.4*	*−3.0*	*−1.3*	5.1
	PN	1.8	4.1	4.6	7.5	9.8	19.8	*−0.9*	−1.0	−0.3	1.4	5.4	10.2
	PT	*−1.8*	2.0	3.0	5.4	7.9	19.9	*−6.8*	*−4.3*	*−4.6*	*−2.5*	3.5	0.0
NCAR	BC	11.2	14.0	14.8	11.6	11.9	15.4	17.3	22.0	20.6	21.8	19.4	3.5
	HM	2.2	5.9	11.4	7.2	7.1	11.5	6.6	11.2	12.5	11.0	8.1	*−2.0*
	HS	11.1	15.2	16.5	12.0	13.5	15.2	18.3	26.2	28.9	27.8	21.1	4.4
	LN	10.2	9.1	12.3	7.9	8.0	8.5	15.2	19.7	19.1	20.1	14.6	9.7
	PN	15.1	15.6	14.7	12.3	13.2	14.7	20.3	22.4	22.7	22.3	16.7	*−0.1*
	PT	10.9	13.2	13.5	10.7	11.5	13.3	14.0	16.7	18.1	18.0	13.4	*−8.7*

not repeated by the other models. Whilst five models project declines in high flows for the Mun, BC projects a small increase. The same model simulates modest declines in high flows at Phnom Penh. Uncertainty in the direction of change in Q5 for MPI is limited to Chiang Saen (and in one case Vientiane). Elsewhere Q5 increases and the magnitude of these changes tends to increase in a downstream direction. Changes in low flows vary; BC, HS and PN project increases throughout the Mekong below Chiang Saen whilst the other models simulate declines at most gauging stations on the main Mekong. All models project increases in Mun low flows.

4. Discussion

This study demonstrates considerable differences in baseline potential evapotranspiration totals (but some consistent spatial and temporal patterns) for the Mekong evaluated using six different, but widely used, PET methods. Without PET observations across the Mekong it is not possible to state whether one method (and hence MIKE SHE model) should be preferred over another (e.g. Prudhomme and Williamson, 2013). It might be expected that PN should produce most realistic results as it incorporates the most meteorological variables, but as previously noted the additional variables are typically relatively poorly observed. Furthermore, net radiation in PN (and PT) is derived empirically from cloud cover data, and only climatological values for wind speed have been used. Although these substitutions are commonly made in large-scale modelling (e.g. Arnell, 2003), their influence on the reliability of PET calculations remains a matter for further research. In the absence of a definitive assessment of the reliability of each PET method, it is at least worth noting that the relative order of magnitude in baseline PET has similarities with previous studies. For example, Kingston et al. (2009) showed that for the latitudinal range of the Mekong, PT consistently produced the lower PET totals whilst the highest PET was for HM and then BC.

Consistent calibration/validation procedures result in alternative parameter values for the six MIKE SHE models which act to mitigate the differences in absolute PET. Each model simulates very similar baseline river discharge and performance is generally "excellent" or "very good". However, results do suggest that the impact of alternative meteorological input distributions, as well

as different precipitation datasets (e.g. CRU TS 3.0), should be investigated. Similarly assessments of the impact of land cover change, including sensitivity associated with alternative PET methods, would merit further exploration.

In the simulation of GCM scenarios, the models are largely sensitive to changes between baseline and scenario PET rather than inter-PET method differences in baseline PET, a positive outcome given the aim of this study. Alternative approaches, such as employing alternative PET data within a model calibrated using a specific PET method, should be interpreted with caution, as has been demonstrated when applying different precipitation datasets to hydrological models (Mileham et al., 2008; Xu et al., 2010).

Inter-GCM ranges of change in PET are small in comparison to those for precipitation. PET increases for all GCMs whilst precipitation climate change signals vary between catchment-wide increases or decreases to spatially variable changes. PET methods with similar inputs (i.e. mean temperature: BC, LN) produce similar baseline values, but markedly different climate change signals. This indicates that the PET equation itself can be just as important a source of uncertainty as the input meteorological variables. The hierarchy of changes in annual PET for a given GCM using different methods is similar to those demonstrated in other studies. Bae et al. (2011) showed that for a range of climate change scenarios, HS consistently produced the lowest change in PET. PT produced larger changes, with the largest due to HM. Kingston et al. (2009) demonstrated that for the latitudinal range of the Mekong, HM also produced the largest changes in PET for five scenarios employed in the current study (CSIRO and HadGEM1 were excluded). Some of the smallest changes were associated with HS PET.

Some consistencies in the relative order of change in annual PET for the different GCMs are also common to other studies. NCAR followed by HadGEM1 produced the smallest increases over three sub-catchments of the Manipur River in northeast India, around 500 km to the west of the Mekong and at the same latitude as central parts of the Lancang (Singh et al., 2010). The largest increases were similarly associated with CSIRO and then HadCM3.

It is important to recognise that whilst this study illustrates the impacts of GCM structural uncertainty on precipitation and PET (and when used within the MIKE SHE models, river discharge) an ensemble of GCMs does not provide a systematic assessment of true GCM structural uncertainty. An alternative is the use of GCM perturbed physics ensembles (PPEs), such as the QUMP ensemble (Murphy et al., 2009). The use of PPEs in climate impact assessments is still a relatively new development (Gosling et al., 2012) but could be employed to extend this research on the Mekong (and other catchments).

PET method-related uncertainty in simulation of river discharge under climate change is considerably less than GCM-related uncertainty (that is in turn dominated by uncertainty in precipitation). It is worth noting, however, that for those scenarios involving a spatially variable precipitation climate change signal, PET method influences the spatial extent of increases or decreases in mean discharge. In these cases, PET specific differences in the direction of change in discharge could have important implications including variability in projected impacts for power generation from existing and planned dams, as well as environmental conditions within the river (e.g. Thompson et al., 2013b).

The finding that the models using alternative PET methods result in some differences in scenario discharge supports the assertion made by Thompson et al. (2013a) that differences in the climate change discharge/runoff signals for the Mekong simulated by MIKE SHE, SLURP and Mac-PDM.09 for the same scenarios could, at least in part, be attributable to PET method (LN for MIKE SHE and SLURP, Penman–Monteith for Mac-PDM.09). However, some increases simulated by the global hydrological model at upstream gauging stations were three to five times as large as those simulated by the catchment models. Such large inter-PET method differences are rare in the current study. Further downstream, however, differences between MIKE SHE/SLURP and Mac-PDM.09 were comparable to those identified herein.

5. Conclusions

Potential evapotranspiration for sub-catchments of the Mekong varies considerably when evaluated using different methods. Priestley–Taylor followed by Hargreaves–Samani and Penman characteristically provide lower PET totals than the Linacre and Blaney–Criddle temperature-based methods. Calibration of six MIKE SHE models each employing different PET data is possible through modification of parameters that act to mitigate the impacts of variations in baseline PET. The performance of each model is very similar, generally being classed as ''excellent'' or ''very good'', and is superior to other models of the Mekong.

Inter-GCM variations in projected changes in precipitation for a prescribed 2 °C increase in global mean temperature are much larger than the corresponding variability in PET changes. In percentage terms, the ranges of change in precipitation are between 2.5 and 10 times as large as those for PET. Whilst PET increases for all GCMs, precipitation changes include catchment-wide increases or decreases, as well as spatially variable directions of change. There is some consistency in projections of change in PET for the different GCMs and PET methods. The largest PET changes are, in general, associated with CSIRO and CCCMA and the smallest with NCAR. For any given GCM, Blaney–Criddle and Hargreaves–Samani produce the smallest changes in PET with the largest resulting from Linacre and Hamon.

Although PET method has some impact on simulated discharge, GCM-related uncertainty for change in mean discharge is, on average, 3.5 times as large as PET method-related uncertainty. In most cases, scenarios associated with catchment-wide increases (decreases) in precipitation produce increases (decreases) in mean discharge irrespective of PET method. The magnitude of changes in discharge is, however, related to PET method, with larger increases (smaller declines) occurring for methods producing the smallest increases in PET (Blaney–Criddle and Hargreaves–Samani). Uncertainty in the direction of change in mean discharge due to PET method occurs for scenarios with spatially variable changes in precipitation. The inter-PET method range of change is, however, relatively small and differences in the direction of change are often limited to a few gauging stations. Greater PET method-related uncertainty in the direction of change in high and low flows is evident, although differences are not sufficient to modify the seasonal distribution of discharge resulting from each scenario. Although choice of PET method has some impact on climate change related projections of future Mekong River discharge, the larger source of uncertainty is due to the choice of GCM and its impact on precipitation.

Acknowledgements

This study develops earlier research supported by a grant from the UK Natural and Environmental Research Council under the Quantifying and Understanding the Earth System (QUEST) programme (Ref. NE/E001890/1). ClimGen climate scenarios were generated by Tim Osborn at the Climatic Research Unit of the University of East Anglia. MIKE SHE model development benefitted from discussions with Mike Butts and Douglas Graham (DHI). We thank Jon French and three anonymous reviewers for their comments and suggestions that led to the improvement of the paper.

References

Alcamo, J., Flörke, M., Märker, M., 2007. Future long-term changes in global water resources driven by socio-economic and climatic changes. Hydrol. Sci. J. 52, 247–275.

Al Khudhairy, D., Thompson, J.R., Gavin, H., Hamm, N.A.S., 1999. Hydrological modelling of a drained grazing marsh under agricultural land use and the simulation of restoration management scenarios. Hydrol. Sci. J. 44, 943–971.

Allen, R.G., Pereira, L.S., Raes, D., Smith, M., 1998. Crop evapotranspiration – Guidelines for computing crop water requirements, FAO Irrigation and Drainage Paper 56. FAO, Rome.

Andersen, J., Refsgaard, J.C., Jensen, K.H., 2001. Distributed hydrological modelling of the Senegal River Basin – model construction and validation. J. Hydrol. 247, 200–214.

Andréasson, J., Bergström, S., Carlsson, B., Graham, L.P., Lindström, G., 2004. Hydrological change: climate change impact simulations for Sweden. Ambio 33, 228–234.

Arnell, N.W., 1999a. The effect of climate change on hydrological regimes in Europe: a continental perspective. Glob. Environ. Change 9, 5–23.

Arnell, N.W., 1999b. A simple water balance model for the simulation of streamflow over a large geographic domain. J. Hydrol. 217, 314–335.

Arnell, N.W., 2003. Effects of IPCC SRES* emissions scenarios on river runoff: a global perspective. Hydrol. Earth Syst. Sci. 7, 619–641.

Arnell, N.W., Osborn, T., 2006. Interfacing Climate and Impacts Models in Integrated Assessment Modelling, Tyndall Centre for Climate Change Research Technical Report 52. Tyndall Centre for Climate Change Research, Southampton and Norwich.

Arnell, N.W., Gosling, S.N., 2013. The impacts of climate change on river flow regimes at the global scale. J. Hydrol. 486, 351–364.

Arnold, J.G., Srinivasan, R., Muttiah, R.S., Williams, J.R., 1998. Large area hydrologic modeling and assessment part I: model development. J. Am. Water Resour. Assoc. 34, 73–89.

Bae, D.H., Jung, I.W., Lettenmaier, D.P., 2011. Hydrologic uncertainties in climate change from IPCC AR4 GCM simulations of the Chungju Basin, Korea. J. Hydrol. 401, 90–105.

Bates, B.C., Kundzewicz, Z.W., Wu, S., Palutikof, J.P. (Eds.), 2008. Climate Change and Water, Technical Paper of the Intergovernmental Panel on Climate Change. IPCC Secretariat, Geneva.

Brouwer, C., Heibloem, M., 1986. Irrigation Water Management: Irrigation Water Needs, Irrigation Water Management Training Manual 3. FAO, Rome.

Carsel, R.F., Parrish, R.S., 1988. Developing joint probability distributions of soil water retention characteristics. Water Resour. Res. 24, 755–769.

Chow, V.T., 1959. Open Channel Hydraulics. McGraw-Hill, New York.

Chun, K.P., Wheater, H.S., Onof, C.J., 2009. Streamflow estimation for six UK catchments under future climate scenarios. Hydrol. Res. 40, 96–112.

Clapp, R.B., Hornberger, G.M., 1978. Empirical equations for some soil hydraulic properties. Water Resour. Res. 14, 601–604.

Conway, D., Hulme, M., 1996. The impacts of climate variability and future climate change in the Nile Basin on water resources in Egypt. Int. J. Water Resour. Dev. 12, 277–296.

Dent, M.C., Schultze, R.E., Angus, G.R. 1988. Crop water requirements, deficits and water yield for irrigation planning in southern Africa. Report 118/1/88. Water Research Commission, Pretoria.

DHI, 2009. MIKE SHE Technical Reference. DHI Water and Environment, Hørsholm.

Dibike, Y.B., Coulibaly, P., 2005. Hydrologic impact of climate change in the Saguenay watershed: comparison of downscaling methods and hydrologic models. J. Hydrol. 307, 145–163.

Döll, P., Kaspar, F., Lehner, B., 2003. A global hydrological model for deriving water availability indicators: model tuning and validation. J. Hydrol. 270, 105–134.

FAO, 1990. FAO-UNESCO Soil Map of the World: Revised Legend, World Soil Resources Report 60. Food and Agriculture Organization of the United Nations, Rome.

Feyen, L., Vázquez, R., Christiaens, K., Sels, O., Feyen, J., 2000. Application of a distributed physically-based hydrological model to a medium size catchment. Hydrol. Earth Syst. Sci. 4, 47–63.

Floch, P. Molle, F. 2007. Marshalling Water Resources: A Chronology of Irrigation Development in the Chi-Mun River Basin Northeast Thailand. CGIAR Challenge Program on Water and Food, Colombo.

Garbrecht, J., Martz, L.W., 1997. TOPAZ Version 1.20: An Automated Digital Landscape Analysis Tool for Topographic Evaluation, Drainage Identification, Watershed Segmentation and Subcatchment Parameterization – Overview. Report number GRL 97–2. USDA Grazinglands Research Laboratory, Agricultural Research Service, El Reno.

Gosling, S.N., 2012. The likelihood and potential impact of future change in the large-scale climate-earth system on ecosystem services. Environ. Sci. Policy 27 (Suppl.), S15–S31.

Gosling, S.N., Arnell, N.W., 2011. Simulating current global river runoff with a global hydrological model: model revisions, validation and sensitivity analysis. Hydrol. Process. 25, 1129–1145.

Gosling, S.N., Bretherton, D., Haines, K., Arnell, N.W., 2010. Global hydrology modelling and uncertainty: running multiple ensembles with a campus grid. Philos. Trans. R. Soc. A 368, 1–17.

Gosling, S.N., McGregor, G.R., Lowe, J.A., 2012. The benefits of quantifying climate model uncertainty in climate change impacts assessment: an example with heat-related mortality change estimates. Clim. Change 112, 217–231.

Gosling, S.N., Taylor, R.G., Arnell, N.W., Todd, M.C., 2011a. A comparative analysis of projected impacts of climate change on river runoff from global and catchment-scale hydrological models. Hydrol. Earth Syst. Sci. 15, 279–294.

Gosling, S.N., Warren, R., Arnell, N.W., Good, P., Caesar, J., Bernie, D., Lowe, J.A., van der Linden, P., O'Hanley, J.R., Smith, S.M., 2011b. A review of recent developments in climate change science. Part II: the global-scale impacts of climate change. Prog. Phys. Geog. 35, 443–464.

Graham, D.N., Butts, M.B., 2005. Flexible, integrated watershed modelling with MIKE SHE. In: Singh, V.P., Frevert, D.K. (Eds.), Watershed Models. CRC Press, Boca Raton, pp. 245–272.

Haddeland, I., Clark, C., Franssen, W., Ludwig, F., Voß, F., Bertrand, N., Folwell, S., Gerten, D., Gomes, S., Gosling, S.N., Hagemann, S., Hanasaki, N., Heinke, J., Kabat, P., Koirala, S., Polcher, J., Stacke, T., Viterbo, P., Weedon, G., Yeh, P., 2011. Multi-model estimate of the global water balance: setup and first results. J. Hydrometeorol. 12, 869–884.

Hagemann, S., Chen, C., Clark, D.B., Folwell, S., Gosling, S.N., Haddeland, I., Hanasaki, N., Heinke, J., Ludwig, F., Voß, F., Wiltshire, A.J., 2012. Climate change impact on available water resources obtained using multiple global climate and hydrology models. Earth Syst. Dyn. Discuss. 3, 1321–1345.

Hapuarachchi, H.A.P., Takeuchi, K., Zhou, M.C., Kiem, A.S., Georgievski, M., Magome, J., Ishidaira, H., 2008. Investigation of the Mekong River basin hydrology for 1980–2000 using the YHyM. Hydrol. Process. 22, 1246–1256.

Hargreaves, G.H., Samani, Z.A., 1982. Estimating potential evapotranspiration. Technical note. J. Irrig. Drain. Eng. - ASCE 108, 225–230.

Havnø, K., Madsen, M.N., Dørge, J., 1995. MIKE 11 – a generalized river modelling package. In: Singh, V.P. (Ed.), Computer Models of Watershed Hydrology. Water Resources Publications, Englewood, pp. 733–782.

Henriksen, H.J., Troldborg, L., Højberg, A.J., Refsgaard, J.C., 2008. Assessment of exploitable groundwater resources of Denmark by use of ensemble resource indicators and a numerical groundwater–surface water model. J. Hydrol. 348, 224–240.

Henriksen, H.J., Troldborg, L., Nyegaard, P., Sonnenborg, T.O., Refsgaard, J.C., Madsen, B., 2003. Methodology for construction, calibration and validation of a national hydrological model for Denmark. J. Hydrol. 280, 52–71.

Huang, Y., Chen, X., Li, Y.P., Willems, P., Liu, T., 2010. Integrated modeling system for water resources management of Tarim River Basin. Environ. Eng. Sci. 27, 255–269.

Hughes, D.A., Kingston, D.G., Todd, M.C., 2011. Uncertainty in water resources availability in the Okavango River basin as a result of climate change. Hydrol. Earth Syst. Sci. 15, 931–941.

Immerzeel, W.W., Pellicciotti, F., Shrestha, A.B., 2012a. Glaciers as a proxy to quantify the spatial distribution of precipitation in the Hunza Basin. Mt. Res. Dev. 32, 30–38.

Immerzeel, W.W., van Beek, P.H., Konz, M., Shrestha, A.B., Bierkens, M.F.P., 2012b. Hydrological response to climate change in a glacierized catchment in the Himalayas. Clim. Change 110, 721–736.

Institute of Hydrology, 1988. Investigation of Dry Season Flows. Water Balance Study Phase 3. Report to the Interim Committee for Coordination of Investigations of the Lower Mekong Basin. Institute of Hydrology, Wallingford.

Ishidaira, H., Ishikawa, Y., Funada, S., Takeuchi, K., 2008. Estimating the evolution of vegetation cover and its hydrological impact in the Mekong River basin in the 21st century. Hydrol. Process. 22, 1395–1405.

Jackson, R.B., Canadell, J., Ehleringer, J.R., Mooney, H.A., Sala, O.E., Schulze, E.D., 1996. A global analysis of root distributions for terrestrial biomes. Oecologia 108, 389–411.

Ji, X., Luo, Y., 2013. The influence of precipitation and temperature input schemes on hydrological simulations of a snow and glacier melt dominated basin in Northwest China. Hydrol. Earth Syst. Sci. Discuss. 10, 807–853.

Kay, A.L., Davies, H.N., 2008. Calculating potential evaporation from climate model data: A source of uncertainty for hydrological climate change impacts. J. Hydrol. 358, 221–239.

Kelliher, F.M., Leuning, R., Schulze, E.D., 1993. Evaporation and canopy characteristics of coniferous forests and grasslands. Oecologia 95, 153–163.

Kiem, A.S., Geogievsky, M.V., Hapaurachchi, H.P., Ishidaira, H., Takeuchi, K., 2005. Relationship between ENSO and snow covered area in the Mekong and Yellow River basins. In: Franks, S.W., Wagener, T., Bøgh, E., Bastidas, L., Nobre, C., Galvão, C.O. (Eds.), Regional Hydrological Impacts of Climate Change – Hydroclimatic variability. IAHS Publ. 296, Wallingford, pp. 255–264.

Kiem, A.S., Ishidaira, H., Hapuarachchi, H.P., Zhou, M.C., Hirabayahi, Y., Takeuchi, K., 2008. Future hydroclimatology of the Mekong River basin simulated using the high-resolution Japan Meteorological Agency (JMA) AGCM. Hydrol. Process. 22, 1382–1394.

Kingston, D.G., Thompson, J.R., Kite, G., 2011. Uncertainty in climate change projections of discharge for the Mekong River Basin. Hydrol. Earth Syst. Sci. 15, 1459–1471.

Kingston, D.G., Todd, M.C., Taylor, R.G., Thompson, J.R., Arnell, N.W., 2009. Uncertainty in the estimation of potential evapotranspiration under climate change. Geophys. Res. Lett. 36, L20403.

Kite, G., 1995. The SLURP model. In: Singh, V.P. (Ed.), Computer models of watershed hydrology. Water Resources Publications, Colorado, pp. 521–562.

Kite, G., 2000. Developing a Hydrological Model for the Mekong Basin: Impacts of Basin Development on Fisheries Productivity. Working Paper 2. International Water Management Institute, Colombo.

Kite, G., 2001. Modelling the Mekong: hydrological simulation for environmental impact studies. J. Hydrol. 253, 1–13.

Kummu, M., Lu, X.X., Wang, J.J., Varis, O., 2010. Basin-wide sediment trapping efficiency of emerging reservoirs along the Mekong. Geomorphology 119, 181–197.
Lacombe, G., Pierret, A., Hoanh, C.T., Sengtaheuanghoung, O., Noble, A.D., 2010. Conflict, migration and land-cover changes in Indochina: a hydrological assessment. Ecohydrology 3, 382–391.
Legates, D.R., Willmott, C.J., 1990. Mean seasonal and spatial variability in gauge-corrected, global precipitation. Int. J. Climatol. 10, 111–127.
Li, S.J., He, D.M., 2008. Water level response to hydropower development in the upper Mekong River. Ambio 37, 170–177.
Lu, J.B., Sun, G., McNulty, S.G., Amataya, D.M., 2005. A comparison of six potential evapotranspiration methods for regional use in the southeastern United States. J. Am. Water Resour. Assoc. 41, 621–633.
Marshall, T.J., Holmes, J.W., Rose, C.W., 1996. Soil Physics, third ed. Cambridge University Press, Cambridge.
Matthews, J.H., Quesne, T.L., 2009. Adapting Water Management: A Primer on Coping with Climate Change. WWF Water Security Series 3, WWF-UK, Godalming.
Meehl, G.A., Covey, C., Delworth, T., Latif, M., McAvaney, B., Mitchell, J.F.B., Stouffer, R.J., Taylor, K.E., 2007. The WCRP CMIP3 Multimodel Dataset: A new era in climate change research. Bull. Am. Meteorol. Soc. 88, 1383–1394.
Mileham, L., Taylor, R.G., Thompson, J.R., Todd, M.C., Tindimugaya, C., 2008. Impact of rainfall distribution on the parameterisation of a soil-moisture balance model of groundwater recharge in equatorial Africa. J. Hydrol. 359, 46–58.
Mitchell, T.D., Jones, P.D., 2005. An improved method of constructing a database of monthly climate observations and associated high-resolution grids. Int. J. Climatol. 25, 693–712.
Murphy, J.M., Sexton, D.M.H., Jenkins, G.J., Boorman, P.M., Booth, B.B.B., Brown, C.C., Clark, R.T., Collins, M., Harris, G.R., Kendon, E.J., Betts, R.A., Brown, S.J., Howard, T.P., Humphrey, K.A., McCarthy, M.P., McDonald, R.E., Stephens, A., Wallace, C., Warren, R., Wilby, R., Wood, R.A. 2009. UK Climate Projections Science Report: Climate Change Projections. Met Office Hadley Centre, Exeter.
Nash, I.E., Sutcliffe, I.V., 1970. River flow forecasting through conceptual models. J. Hydrol. 10, 282–290.
Nawaz, N.R., Adeloye, A.J., 2006. Monte Carlo assessment of sampling uncertainty of climate change impacts on water resources yield in Yorkshire, England. Clim. Change 78, 257–292.
New, M., Hulme, M., Jones, P.D., 1999. Representing twentieth century space-time climate variability, Part I: Development of a 1961–1990 mean monthly terrestrial climatology. J. Clim. 12, 829–856.
Nijssen, B., O'Donnell, G.M., Hamlet, A.F., Lettenmaier, D.P., 2001. Hydrologic sensitivity of global rivers to climate change. Clim. Change 50, 143–175.
Nobuhiro, T., Shimizu, A., Kabeya, N., Tamai, K., Ito, E., Araki, M., Kubota, T., Tsuboyama, Y., Chann, S., 2008. Evapotranspiration during the late rainy season and middle of the dry season in the watershed of an evergreen forest area, central Cambodia. Hydrol. Process. 22, 1281–1289.
Nohara, D., Kitoh, A., Hosaka, M., Oki, T., 2006. Impact of climate change on river discharge projected by multimodel ensemble. J. Hydrometeorol. 7, 1076–1089.
Penman, H.L., 1948. Natural evaporation from open water, bare soil and grass. Proc. Roy. Soc. London A 194(Suppl.), 120–145.
Poff, N.L., Brinson, M.M., Day. Jr. J.W., 2002. Aquatic Ecosystems and Global Climate Change. Pew Center on Global Climate Change, Arlington.
Prudhomme, C., Davies, H., 2009. Assessing uncertainties in climate change impact analyses on the river flow regimes in the UK. Part 1: baseline climate. Clim. Change 93, 177–195.
Prudhomme, C., Williamson, J., 2013. Derivation of RCM-driven potential evapotranspiration for hydrological climate change impact analysis in Great Britain: a comparison of methods and associated uncertainty in future projections. Hydrol. Earth Syst. Sci. 17, 1365–1377.
Randall, D.A., Wood, R.A., Bony, S., Colman, R., Fichefet, T., Fyfe, J., Kattsov, V., Pitman, A., Shukla, J., Srinivasan, J., Stouffer, R.J., Sumi, A., Taylor, K.E., 2007. Climate models and their evaluation. In: Solomon, S., Qin, D., Manning, M., Chen, Z., Marquis, M., Averyt, K.B., Tignor, M., Miller, H.L. (Eds.), Climate Change 2007: The Physical Science Basis Contribution of Working Group I to the Fourth Assessment Report of the Intergovernmental Panel on Climate Change. Cambridge University Press, Cambridge and New York, pp. 589–662.
Refsgaard, J.C., Storm, B., Clausen, T., 2010. Système Hydrologique Europeén (SHE): review and perspectives after 30 years development in distributed physically-based hydrological modelling. Hydrol. Res. 41, 355–377.
Sahoo, G.B., Ray, C., De Carlo, E.H., 2006. Calibration and validation of a physically distributed hydrological model, MIKE SHE, to predict streamflow at high frequency in a flashy mountainous Hawaii stream. J. Hydrol. 327, 94–109.
Schultz, R.E., 1989. ACRU: Background, concepts and theory. Report 35, Agricultural Catchments Research Unit, Department of Agricultural Engineering, University of Natal, Pietermaritzburg.
Shopea, N., 2003. Station Profiles of Water Quality Monitoring Network in Cambodia: MRC Water Quality Monitoring Station Network Review. Mekong River Commission, Phnom Penh.
Shuttleworth, W.J., 1993. Evaporation, in: Maidment D.R. (Ed.), Handbook of Hydrology. McGraw-Hill, New York, pp. 4.1–4.53.
Singh, C.R., Thompson, J.R., French, J.R., Kingston, D.G., Mackay, A.W., 2010. Modelling the impact of prescribed global warming on runoff from headwater catchments of the Irrawaddy River and their implications for the water level regime of Loktak Lake, northeast India. Hydrol. Earth Syst. Sci. 14, 1745–1765.
Singh, C.R., Thompson, J.R., Kingston, D.G., French, J.R., 2011. Modelling water-level options for ecosystem services and assessment of climate change: Loktak Lake, northeast India. Hydrol. Sci. J. 56, 1518–1542.
Sperna Weiland, F.C., Tisseuil, C., Dürr, H.H., Vrac, M., van Beek, L.P.H., 2012. Selecting the optimal method to calculate daily global reference potential evaporation from CFSR reanalysis data for application in a hydrological model study. Hydrol. Earth Syst. Sci. 16, 983–1000.
Stisen, S., Jensen, K.H., Sandholt, I., Grimes, D.I.F., 2008. A remote sensing driven distributed hydrological model of the Senegal River basin. J. Hydrol. 354, 131–148.
Stone, R., 2010. Along with power, questions flow at Laos's new dam. Science 328, 414–415.
Thompson, J.R., Gavin, H., Refsgaard, A., Refstrup Sørenson, H., Gowing, D.J., 2009. Modelling the hydrological impacts of climate change on UK lowland wet grassland. Wetlands Ecol. Manag. 17, 503–523.
Thompson, J.R., 2012. Modelling the impacts of climate change on upland catchments in southwest Scotland using MIKE SHE and the UKCP09 probabilistic projections. Hydrol. Res. 43, 507–530.
Thompson, J.R., Green, A.J., Kingston, D.G., Gosling, S.N., 2013a. Assessment of uncertainty in river flow projections for the Mekong River using multiple GCMs and hydrological models. J. Hydrol. 466, 1–30.
Thompson, J.R., Laizé, C.L.R., Green, A.J., Acreman, M.C., Kingston, D.G., 2013b. Climate change uncertainty in environmental flows for the Mekong River. Hydrol. Sci. J. (Online: Author Accepted Version).
Thompson, J.R., Refstrup Sørenson, H., Gavin, H., Refsgaard, A., 2004. Application of the coupled MIKE SHE/MIKE 11 modelling system to a lowland wet grassland in Southeast England. J. Hydrol. 293, 151–179.
Todd, M.C., Taylor, R.G., Osborn, T., Kingston, D., Arnell, N., Gosling, S., 2011. Uncertainty in climate change impacts on basin-scale freshwater resources – preface to the special issue: the QUEST-GSI methodology and synthesis of results. Hydrol. Earth Syst. Sci. 15, 1035–1046.
Västilä, K., Kummu, M., Sangmanee, C., Chinvanno, S., 2010. Modelling climate change impacts on the flood pulse in the Lower Mekong floodplains. J. Water Clim. Change 1, 67–86.
Vázquez, R.F., Feyen, L., Feyen, J., Refsgaard, J.C., 2002. Effect of grid size on effective parameters and model performance of the MIKE SHE code. Hydrol. Process. 16, 355–372.
Vieux, B.E., 2004. Distributed Hydrologic Modeling Using GIS. Kluwer Academic, Dordrecht.
Vörösmarty, C.J., Federer, C.A., Schloss, A.J., 1998. Potential evaporation functions compared on US watersheds: Possible implications for global-scale water balance and terrestrial ecosystem modelling. J. Hydrol. 207, 147–169.
Wang, J.J., Lu, X.X., Kummu, M., 2011. Sediment load estimates and variations in the lower Mekong River. River Res. Appl. 27, 33–46.
Xu, H., Taylor, R.G., Kingston, D.G., Jiang, T., Thompson, J.R., Todd, M., 2010. Hydrological modelling of the River Xiangxi using SWAT2005: a comparison of model parameterizations using station and gridded meteorological observations. Quat. Int. 226, 54–59.
Yan, J., Smith, K., 1994. Simulation of integrated surface water and ground water systems – Model formulation. Water Resour. Bull. 30, 1–12.
Yu, M., Chen, X., Li, L., Bao, A., de la Paix, M.J., 2011. Streamflow simulation by SWAT using different precipitation sources in large arid basins with scarce raingauges. Water Resour. Manage. 25, 2669–2681.